Article

Developmental Cell

The *Arabidopsis* mature endosperm promotes seedling cuticle formation via release of sulfated peptides

Graphical abstract

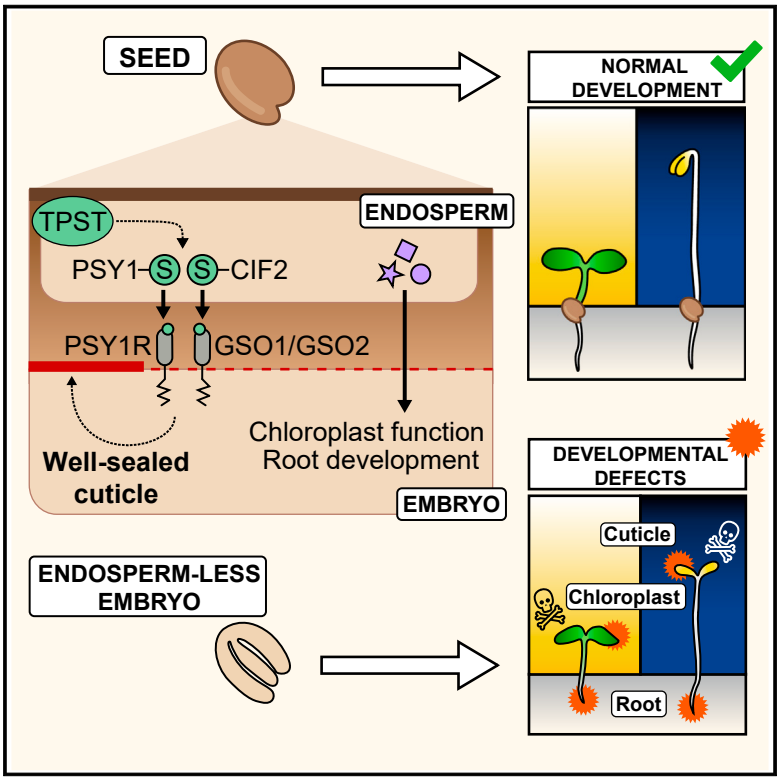

Highlights

- The well-sealed seedling cuticle is formed during the embryo-to-seedling transition
- Endosperm grafting shows that the endosperm promotes seedling cuticle formation
- Endosperm TPST-sulfated CIF2 and PSY1 peptides promote seedling cuticle formation
- Normal seedling development requires developmental signals released by the endosperm

Authors

Julien De Giorgi, Christelle Fuchs, Mayumi Iwasaki, ..., Satoshi Fujita, Sylvain Loubéry, Luis Lopez-Molina

Correspondence

luis.lopezmolina@unige.ch

In brief

De Giorgi et al. show that the embryo-to-seedling developmental transition in *Arabidopsis* is a nonautonomous process dependent on factors released by the endosperm. The authors focus on seedling cuticle development and show, using an endosperm grafting technique, that the endosperm peptides CIF2 and PSY1 promote cuticle formation.

De Giorgi et al., 2021, Developmental Cell *56*, 3066–3081
November 22, 2021
https://doi.org/10.1016/j.devcel.2021.10.005

CellPress

CellPress
OPEN ACCESS

Developmental Cell

Article

The *Arabidopsis* mature endosperm promotes seedling cuticle formation via release of sulfated peptides

Julien De Giorgi,[1] Christelle Fuchs,[1] Mayumi Iwasaki,[1] Woohyun Kim,[1] Urszula Piskurewicz,[1] Kay Gully,[2] Anne Utz-Pugin,[1] Laurent Mène-Saffrané,[3] Patrice Waridel,[4] Christiane Nawrath,[2] Fiamma Paolo Longoni,[1,6] Satoshi Fujita,[2,7] Sylvain Loubéry,[1] and Luis Lopez-Molina[1,5,8,*]

[1]Department of Botany and Plant Biology, University of Geneva, Geneva, Switzerland
[2]Department of Plant Molecular Biology, University of Lausanne, Lausanne, Switzerland
[3]Department of Biology, University of Fribourg, 1700 Fribourg, Switzerland
[4]Protein Analysis Facility, University of Lausanne, Lausanne, Switzerland
[5]Institute of Genetics and Genomics in Geneva (iGE3), University of Geneva, Geneva, Switzerland
[6]Present address: Laboratory of Plant Physiology, Faculty of Sciences, Institute of Biology, University of Neuchâtel, Neuchâtel, Switzerland
[7]Present address: National Institute of Genetics (NIG), Yata 1111, Mishima, Shizuoka 411-8540, Japan
[8]Lead contact
*Correspondence: luis.lopezmolina@unige.ch
https://doi.org/10.1016/j.devcel.2021.10.005

SUMMARY

In *Arabidopsis* mature seeds, the onset of the embryo-to-seedling transition is nonautonomously controlled, being blocked by endospermic abscisic acid (ABA) release under unfavorable conditions. Whether the mature endosperm governs additional nonautonomous developmental processes during this transition is unknown. Mature embryos have a more permeable cuticle than seedlings, consistent with their endospermic ABA uptake capability. Seedlings acquire their well-sealing cuticles adapted to aerial lifestyle during germination. Endosperm removal prevents seedling cuticle formation, and seed reconstitution by endosperm grafting onto embryos shows that the endosperm promotes seedling cuticle development. Grafting different endosperm and embryo mutant combinations, together with biochemical, microscopy, and mass spectrometry approaches, reveal that the release of tyrosylprotein sulfotransferase (TPST)-sulfated CIF2 and PSY1 peptides from the endosperm promotes seedling cuticle development. Endosperm-deprived embryos produced nonviable seedlings bearing numerous developmental defects, not related to embryo malnutrition, all restored by exogenously provided endosperm. Hence, seedling establishment is nonautonomous, requiring the mature endosperm.

INTRODUCTION

Mature seeds are metabolically inert and highly resistant structures favoring plant dispersal (Baroux and Grossniklaus, 2019). In angiosperms, seed development is initiated after a double-fertilization event that produces the endosperm and zygote. Thereupon, the zygote undergoes embryogenesis followed by maturation where the seed accumulates food stores, to fuel future seedling development, and desiccates. The endosperm is a nourishing tissue of unclear evolutionary origin, developing alongside the embryo prior to the formation of the mature seed (Baroux et al., 2002).

In persistent endosperm species, such as cereals, the endosperm occupies the largest volume of mature seeds where it stores food for future seedling establishment (Baroux and Grossniklaus, 2019). In contrast, in non-persistent endosperm species, the endosperm may be absent from mature seeds, as in the orchid family, or be present as a minor component, as in the economically important Brassicaceae or Fabaceae families, which mainly store food in the embryo (Baroux and Grossniklaus, 2019). The latter case raises the question of the biological function of the endosperm in mature seeds of non-persistent endosperm species. The mature seed of the Brassicaceae *Arabidopsis thaliana* consists of an outer dead seed coat (testa) arising from ovular integuments, underneath which a single layer of mature endosperm live cells surround the mature embryo.

The onset of the embryo-to-seedling transition is a decisive moment for plant survival. There are different mechanisms controlling seed germination. For example, newly produced seeds are dormant, i.e., they will not germinate even under favorable germination conditions. Dormancy is imposed by the mature endosperm, which releases abscisic acid (ABA) toward the embryo to block its growth and maintain its stress-resistant embryonic state (Ali-Rachedi et al., 2004; Bethke et al., 2007; Lee et al., 2010; Kinoshita et al., 2010; Lopez-Molina et al., 2002). The endosperm continues to control germination in non-dormant

seeds as it releases ABA under unfavorable conditions (Lee et al., 2012; Piskurewicz and Lopez-Molina, 2016).

The evolutionary forces leading to the control of seed germination by the mature endosperm are unknown and intriguing. Whether the mature endosperm governs additional developmental processes before or during the embryo-to-seedling transition is unknown. Here, we asked (1) whether embryonic uptake of endospermic ABA imposes developmental constraints to the mature embryo, (2) whether these constraints are compatible with viable seedling formation, if left unresolved, and (3) whether the endosperm plays a role in their resolution.

During the embryo-to-seedling transition, two key processes take place. Undifferentiated plastids in the embryo import thousands of proteins to rapidly assemble the photosynthetic apparatus and form chloroplasts, which is essential to render seedlings autotrophic (Jarvis and López-Juez, 2013). The root stem cells start dividing and differentiating to establish a functional root meristematic zone, which is essential for primary root growth (Petricka et al., 2012).

The plant cuticle is a hydrophobic layer of lipids with the polyester cutin, consisting of C16 and C18 oxygenated fatty acids, as a major component, as well as aliphatic waxes impregnating the cuticle that covers primary plant organs and forms a diffusion barrier regulating fluxes of molecules between different organs, as well as the environment. Cuticular wax has a very different structure, composition, and properties even within the same plant and even among different developmental stages of the same organ (Jeffree, 2006; Nawrath et al., 2013). The cuticle is already laid down early during embryogenesis around the globular stage and expands with the growth of the plant being constantly restructured during development to the needs of the local environment (Berhin et al., 2019; Fabre et al., 2016; Szczuka and Szczuka, 2003). During the embryo-to-seedling transition, the mature embryo surrounded and protected by seed coat, suddenly faces much more variable environmental conditions and requires protection against drought, waterlogging, microorganisms, and other stresses (Ingram and Nawrath, 2017; Lee et al., 2021).

A previous report showed that toluidine blue O (TBO) uptake in mature embryos occurs after a few seconds of exposure to the dye, unlike in seedlings where TBO uptake remains limited even after several minutes (De Giorgi et al., 2015). This suggests that the mature embryo and seedling cuticle do not have the same properties. A more permeable cuticle in the embryo than in seedlings is consistent with endospermic ABA uptake by the embryo for the control of seed germination. Furthermore, a previous report showed that repression of embryonic growth by ABA is limited in time upon seed imbibition, ending after seed germination so that seedling establishment is no longer prevented by ABA (Lopez-Molina et al., 2001). Reduced response to ABA could reflect reduced ABA uptake by the plant due to the restructuration of the mature embryo cuticle during the embryo-to-seedling transition to equip seedlings with a well-sealed cuticle.

Here, we show that the seedling cuticle is progressively formed shootwards during the embryo-to-seedling transition, gaining better sealing properties suitable for the seedling's life in aerial conditions. We show that the sealing, i.e., the organization of the seedling cuticle, is a nonautonomous process that depends on the mature endosperm, as shown by a grafting technique. Grafting mature endosperms and mature embryos of different genetic backgrounds, together with transmission electron microscopy (TEM), mass spectrometry, and pharmacological studies, reveals a model whereby sulfated peptide release by the mature endosperm promotes cuticle restructuration in the epidermis of embryos as they emerge from the seed. Furthermore, and surprisingly, we found that seedling chloroplast and root development is also nonautonomous, critically requiring diffusible compounds released by the mature endosperm in a manner not related to food supply.

RESULTS

The seedling cuticle is formed during the embryo-to-seedling transition

We explored the formation of the seedling cuticle, including the mechanism leading to its strong sealing properties required for its aerial life upon emergence from the seed. Changes in cuticle permeability were monitored by staining with TBO. Torpedo and mature-stage embryos had high TBO uptake relative to newly emerged seedlings (Figures 1A and S1A) (STAR Methods). Upon seed germination, the emerged hypocotyl had low TBO uptake, whereas the still un-emerged cotyledons, i.e., cotyledons still surrounded by the endosperm, had high TBO uptake. After their emergence, cotyledons had acquired low TBO uptake so that the entire seedling, with the exception of the juvenile primary root, had low TBO uptake, consistent with previous reports (Figures 1A and S1A) (Tanaka et al., 2004). These observations reveal that the embryo cuticle progressively acquires low permeability during the embryo-to-seedling transition.

We studied the cuticle structure in torpedo, mature embryo, and fully emerged seedlings by TEM (STAR Methods). We identified three main cuticle categories, present in all developmental stages, labeled as "thin interface," "thick interface," and "diffuse." In the "thin interface" category, the cuticle proper, composed of a darker osmiophilic inner band and a lighter less osmiophilic outer band, was located between a thin cell wall-cuticle interface and an electron-opaque outer layer (Figure 1B) (Bourgault et al., 2020; Jeffree, 2006). Category "thick interface" had a thicker electron-opaque band at the cuticle interface and the dark inner band of the cuticle proper (Figure 1B). Category "diffuse" had a single, thick, electron-opaque band on the outer side of the cell wall, compromising the unambiguous identification of the different cuticle layers (Figure 1B). A series of TEM photographs taken along the cotyledon epidermis at different developmental stages were used to measure the length occupied by each cuticle category and to calculate its relative contribution to the cuticle (STAR Methods) (Figure S1B). For each developmental stage, we did not observe that a given cuticle category was overrepresented in the epidermal cells of a given region along the cotyledon epidermis, and two or three cuticle categories could be found in a given TEM photograph (Figure S1C). The cuticle observed in the torpedo and mature embryo stages was structurally distinct from that of seedlings. The "thin interface" category was predominant (80% median contribution) in seedlings, whereas it was less frequent in torpedo and mature embryos (53%–42%) where the "diffuse" category was markedly more frequent than in seedlings (30%–47% versus 5%) (Figure 1C). These results corroborate the notion that the cuticle undergoes a remarkable modification during the embryo-to-seedling transition.

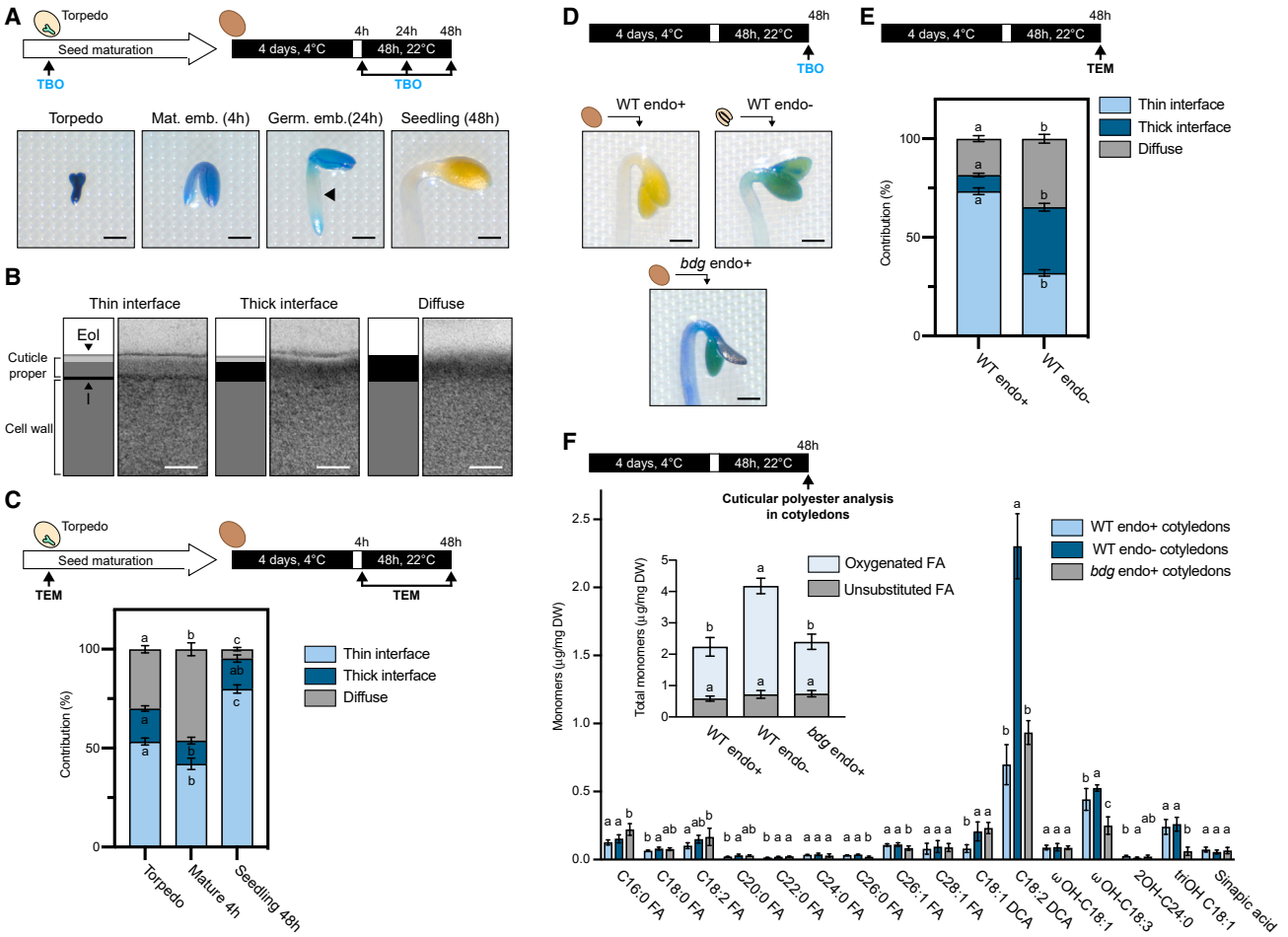

Figure 1. Seedling cuticle formation occurs after germination and requires the mature endosperm

Diagrams depict the procedures to obtain plants at different developmental stages during the embryo-to-seedling transition prior to TBO uptake assays, TEM or polyester quantification, as indicated.

(A) Representative pictures of WT torpedo (torpedo) embryos, mature embryos (4 h), germinated embryos (24 h), and seedlings (48 h) processed together in a TBO uptake assay (bars, 0.2 mm). Arrowhead at 24 h indicates differences in TBO uptake.

(B) TEM pictures illustrating the "thin interface," "thick interface," and "diffuse" cuticle categories (bars, 500 nm). EoI, electron-opaque outer layer; I, cell wall-cuticle interface.

(C) Cuticle categories contributions (%) to the WT cotyledon epidermis cuticle observed by TEM in torpedo, mature embryo (4 h), and seedling (48 h) stages. Data represent the mean ± SEM (three biological replicates, n = 134–173 pictures). Statistically significant differences between the different conditions are indicated by different letters as assessed by Kruskal-Wallis tests followed by post-hoc Dunn's tests ($p < 0.05$).

(D) Representative pictures of WT endo+ and endo− seedlings processed together in a TBO uptake assay. *bdg* endo+ seedlings are shown as a reference (bars, 0.3 mm).

(E) Cuticle categories contributions (%) in WT endo+ and endo− cotyledons. Data represent the mean ± SEM (three biological replicates, n = 237–241 pictures). Statistical differences as assessed by Mann-Whitney test ($p < 0.0001$).

(F) Quantification of cutin monomers and the total cutin amount (insert) present in dissected cotyledons of WT endo+ and endo− seedlings. Statistically significant differences between the different genotypes are indicated by different letters as assessed by a two-way ANOVA test followed by a post-hoc Tukey test, ($p < 0.05$, two biological replicates, n = 4–8).

Presence of the mature endosperm is necessary for seedling cuticle formation

To investigate the role of the mature endosperm for seedling cuticle formation and other seedling developmental processes, the seed's testa and endosperm were removed together from the mature seed 4 h after its imbibition (Figure S1D). The resulting endosperm-less embryos are hereafter referred to as "endo− embryos" and the seedlings they develop into as "endo− seedlings" (Figure S1D). Tissues from endo− seedlings were given an "endo−" label; e.g., "endo− cotyledons." Non-manipulated plant material was given an "endo+" label. Unless specified otherwise, endo− and endo+ seedlings were studied 48 h after the end of seed stratification, which was a time where endo+ seedlings have fully emerged from the seed (Figure S1D) (STAR Methods).

Strikingly, TBO uptake was high in endo− seedlings relative to endo+ seedlings, particularly in the cotyledons, being less elevated than that of the cuticle-defective *bdg* mutants (Figures

1D and S1E) (Kurdyukov et al., 2006). Unlike endo+ seedlings, the cotyledon cuticle of endo− seedlings did not have a predominant "thin interface" category but instead had an increase in the "thick interface" and "diffuse" categories (Figure 1E). These results indicated that seedling cuticle formation requires the presence of the mature endosperm between the time of seed imbibition and seed germination.

Cotyledons of endo− seedlings have an abnormal cuticular polyester content

To corroborate this claim, we characterized the polyester content of the endo− cotyledon cuticle by measuring the abundance of esterified lipids and aromatic acids in dissected cotyledons of endo+ and endo− seedlings. Strikingly, we found that the most abundant oxygenated monomers of cutin in WT endo+ cotyledons, α, ω-octadecenoic acid (C18:2 DCA), was increased by 3.3-fold in WT endo− cotyledons (Figure 1F). Furthermore, WT endo− cotyledons also had a 2.5-fold increase in α, ω-octadecadiendioic acid (C18:1 DCA) levels. Overall, oxygenated polyester monomer levels were increased by about 2-fold in the WT endo− cuticle, whereas the unsubstituted polyester monomer levels were unaltered (Figure 1F). A higher amount of polyester content in the cuticle, together with the higher permeability of the cuticle, is likely caused by misregulation of the cutin biosynthetic pathway, leading to a misbalance of the cuticular components that cannot form a well-sealing cuticle, as it has been seen in cuticles of several *Arabidopsis* mutants, such as the cuticle of 5-weeks-old rosette leaves of *lcr* and *bdg* (Kurdyukov et al., 2006; Voisin et al., 2009).

As a reference, we also analyzed the polyester composition of the cuticle-defective *bdg* endo+ cotyledons. We found that particular polyester monomers were changed in *bdg* endo+ cotyledons relative to WT endo+ cotyledons, notably, 9,10,18-trihydroxy octadecenoic acid (triOH-C18:1) and omega-hydroxy-C18:3 (ωOH-C18:3) were reduced by about 4-fold and 1.7-fold, respectively, whereas α, ω-octadecenoic acid (C18:1 DCA) was increased by about 3-fold. However, overall, the total amount of oxygenated polyester compounds did not change in *bdg* endo+ cotyledons relative to WT (Figure 1F). A reduction of in-chain hydroxylated FAs has also been seen in rosette leaves of 21-day-old *bdg* plants, whereas increased amounts of C18:1 DCA have been seen in older rosette leaves of *bdg*. Cutin composition and amount changes strongly during development in the *bdg* mutant, likely because of the activation of a compensation mechanism in response to the primary deficiency in cutin biosynthesis (Jakobson et al., 2016; Kurdyukov et al., 2006).

These measurements show that the biosynthesis and deposition of cuticular polyester material is defective in WT endo− cotyledons. Improper cuticle formation in endo− seedlings could reflect the stress imposed by endosperm removal. However, improper cuticle formation was not observed when the endosperm was removed soon after germination when most of the embryo remains surrounded by the endosperm, which entails a similar stress as with non-germinated seeds (Figure S1F).

Together, these results lead us to conclude that (1) mature embryos have a cuticle that is distinct from that of seedlings, (2) the seedling cuticle is formed during the mature embryo-to-seedling transition, and (3) the mature endosperm is needed for seedling cuticle formation. We also noticed that endo− seedlings developed severe developmental defects, which will be further described later on.

Grafting dissected mature embryos with mature endosperm restores seedling cuticle formation

A "seed coat bedding" assay (SCBA), whereby endo− embryos are cultured on a bed of dissected mature endosperms with the seed coat (testa) still attached, enables studying endo− embryo development under the influence of the underlying endosperm (Lee and Lopez-Molina, 2013). Strikingly, WT endo− embryos cultured on a bed of WT mature endosperms/testa (SCBA) for 48 h produced endo− seedlings that had a low uptake of TBO, similar to that of endo+ seedlings (Figure S2A). A SCBA using only dissected testas did not lower TBO uptake, unlike a SCBA using endosperm only (Figure S2A). Interestingly, we noticed that 24 h after stratification, cotyledons and hypocotyls in a SCBA started acquiring low TBO uptake simultaneously, unlike endo+ seedlings where low TBO uptake acquisition proceeds shootwards during the embryo-to-seedling transition (Figures 1A and S2B). As little as 5 endosperms could lower TBO uptake in endo− seedlings, which prompted us to graft a single endosperm tissue, with the testa still attached, onto an endo− embryo so as to closely mimic the natural seed configuration (STAR Methods) (Figures 2A and S2C). We also developed a cotyledon image warping protocol to perform statistical analysis of TBO uptake throughout the surface of cotyledons of varying sizes and shapes. This also enables diluting out high-intensity blue staining signals corresponding to local wounds arising from the dissection procedure, which compromises whole cotyledon TBO uptake quantification (STAR Methods) (Figures 2B and S2D). Remarkably, grafting an individual WT mature endosperm onto a WT endo− embryo was able to markedly lower TBO uptake throughout the surface of endo− cotyledons relative to ungrafted endo− cotyledons, without, however, fully achieving the low TBO uptake of endo+ seedlings (Figure 2B). Furthermore, and strikingly, grafted endo− seedlings recovered a cuticle reminiscent of that of endo+ seedlings with a marked increase in the contribution of the "thin interface" category and a significant decrease in that of the "thick interface" and "diffuse" categories (Figure 2C). Nevertheless, the rescued cuticle remained statistically significantly different relative to endo+ seedlings with the exception of the "diffuse" category (Figure 2C). Altogether, these results show that the mature endosperm promotes seedling cuticle formation and strongly suggest that it does so through the release of diffusible compounds.

The newly formed seedling cuticle renders embryos less responsive to ABA

A growth arrest checkpoint was previously described whereby exogenously provided ABA elicits a strong embryonic growth arrest prior to germination but not thereafter (Lopez-Molina et al., 2001). We surmised that prior to germination, formation of the seedling cuticle is incomplete, which enables efficient ABA uptake by the embryo, leading to its growth arrest, unlike after germination. The cuticle-deficient *bdg*, *lacs2*, and *gpat4gpat8* mutants showed no obvious germination phenotype under standard germination conditions. As expected, the mutant seeds exposed to ABA did not germinate for 72 h and therefore did not form a seedling similar to WT seeds (Figure S2E). However,

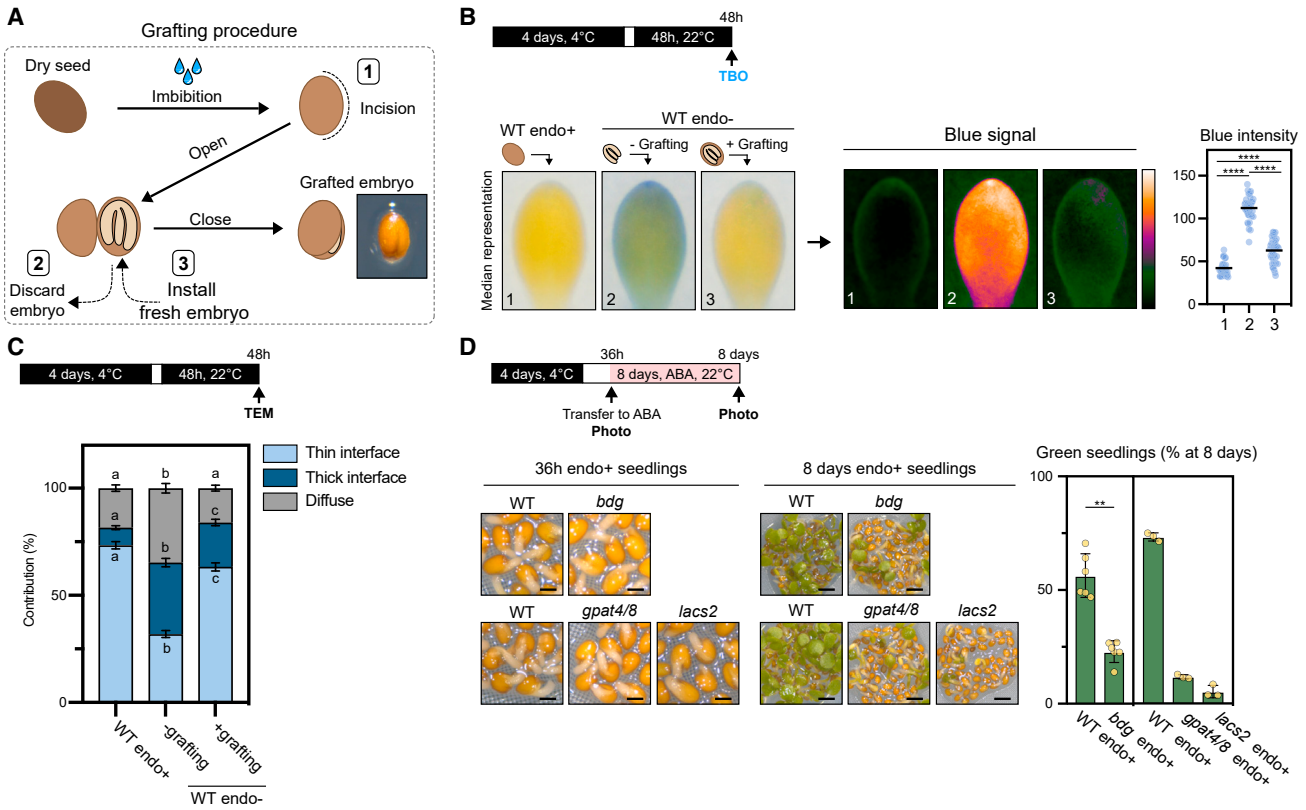

Figure 2. The seedling cuticle requires the endosperm for its formation and reduces seedling responses to ABA

(A) Procedure to graft mature endosperm onto mature embryos. The imbibed seed is incised (1) along the embryonic hypocotyl and the embryo is removed (2) and replaced by a freshly dissected mature embryo (3). The picture shows the recomposed seed after the grafting procedure.

(B) TBO uptake experiments with WT endo+ and endo− seedlings. Images show a median cotyledon representation constructed after warping individual WT endo+ and endo− cotyledon images into an ellipse. Warped cotyledons were stacked, and a median projection was calculated and represented (left row). To better visualize the TBO signal, the red channel of the median representation was inverted (right row), and a look-up table (depicted next to the rightmost image) was applied to discern finer intensity fluctuations. Scatter dot plots show individual and mean (horizontal line) pixel blue color intensity in the warped cotyledons (n = 38–40 cotyledons). Statistical differences as assessed by one-way ANOVA test followed by a post-hoc Tukey test (ns [not significant] $p > 0.05$, *$p \leq 0.05$, **$p \leq 0.01$, ***$p \leq 0.001$; ****$p \leq 0.0001$).

(C) Cuticle categories contributions (%) in WT endo+ cotyledons and WT endo− cotyledons arising from endo− embryos grafted or ungrafted with WT endosperm. Statistics as in Figure 1C (four biological replicates, n = 237–248).

(D) Percentage of green seedlings being formed at 8 days after exposing to ABA (3 μM) WT, *bdg*, *gpat4/gpat8*, and *lacs2* seeds upon their germination 36 h after stratification (36 h). Representative pictures of plant material at each time are shown (bars, 0.3 and 1 mm). Data represent the mean ± SD (*bdg*, two biological replicates, n = 6, *gpat4/gpat8* and *lacs2*: one biological replicate, n = 3). Statistical differences as assessed by Mann-Whitney test.

when seeds were exposed to ABA upon their germination (~36 h after stratification), whereas the majority of WT seeds succeeded to form seedlings, the majority of *bdg*, *lacs2*, and *gpat4gpat8* embryos exhibited strong growth arrest responses to ABA and failed to form seedlings (Figure 2D). These results suggest that after germination, the seedling cuticle limits ABA uptake, thus enabling seedling growth despite the presence of exogenous ABA. They also suggest that the embryonic cuticle is adapted to enable endospermic ABA uptake and thus the control of seed germination by the endosperm.

Tyrosylprotein sulfotransferase (TPST) activity in the endosperm promotes endo– seedling cuticle formation

Sulfate peptide signaling promotes apoplastic barrier formation (Doblas et al., 2017; Nakayama et al., 2017). Peptide sulfation is catalyzed by tyrosylprotein sulfotransferase (TPST), encoded by a single-copy gene (Komori et al., 2009). A recent report showed that newly emerged *tpst-1* (referred as *tpst*) and *sgn2-1* mutant seedlings, lacking a functional *TPST*, display high TBO uptake relative to WT seedlings (Doblas et al., 2017; Doll et al., 2020). Therefore, we investigated the role of sulfated peptide signaling in seedling cuticle formation. We confirmed that *tpst* and *sgn2-1* mutant seedlings have higher TBO uptake relative to WT seedlings (Figures 3A and S3A). TEM analysis did not reveal a specific structural defect in the *tpst* cuticle. Rather, it revealed changes in the relative contribution of each cuticle category reminiscent of that in WT endo− seedlings with a lower contribution of the "thin interface" category and higher contribution of the "thick interface" and "diffuse" categories relative to WT endo+ seedlings (Figure 3B). Unsurprisingly, *tpst* also exhibited hypersensitive responses to ABA after germination (Figure S3B).

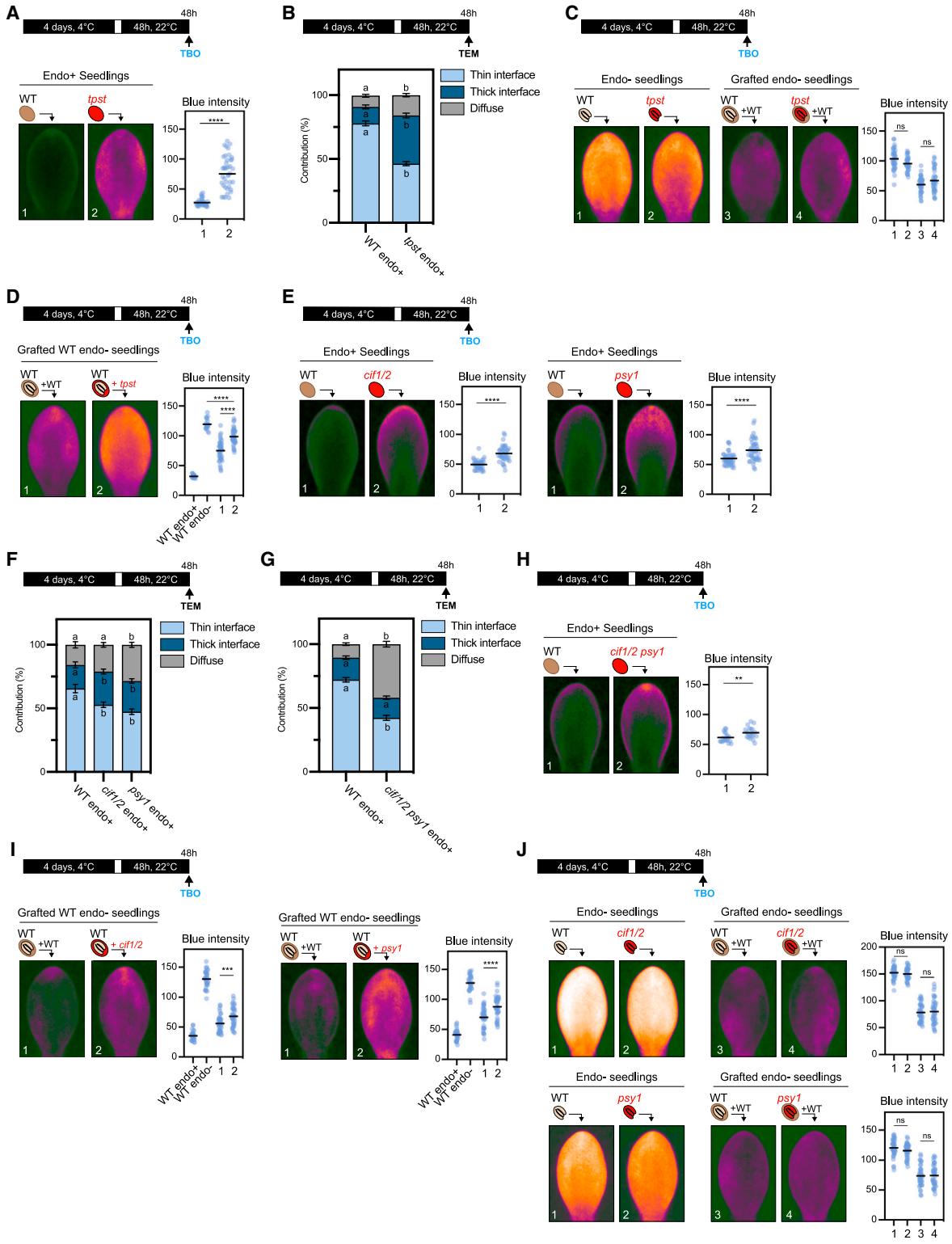

Figure 3. Endospermic TPST, PSY1, and CIF2 promote seedling cuticle formation

TBO uptake quantification and cotyledon imaging using false colors as in Figure 2B.

(A) TBO uptake in WT and *tpst* endo+ seedlings. Data represent the mean (n = 39–40 cotyledons). Statistical differences as assessed by Student's t test.

(B) Cuticle categories contributions (%) in WT and *tpst* endo+ cotyledons. Statistics as in Figure 1E (three biological replicates, n = 186–187).

(C) TBO uptake in WT (1) and *tpst* (2) endo− seedlings and in WT (3) and *tpst* (4) endo− seedlings after grafting WT endosperm onto WT and *tpst* endo− embryos, respectively. Statistics as in Figure 2B (n = 37–40).

(legend continued on next page)

The cuticle defects of *tpst* seedlings could result from a defective activity of the endosperm to promote seedling cuticle formation or an inability of embryos to perceive or process the signals from the endosperm promoting seedling cuticle formation or both. We used the grafting procedure to address these questions. WT and *tpst* endo− cotyledons did not have marked differences in TBO uptake (Figures 3C and S3A). WT and *tpst* endo− seedlings arising from endo− embryos grafted with WT endosperm had similar low TBO uptake (Figures 3C and S3C). These results indicated that embryonic *TPST* is not necessary for seedling cuticle formation. However, and strikingly, WT endo− seedlings arising from endo− embryos grafted with *tpst* endosperm had higher TBO uptake than those grafted with WT endosperm (Figures 3D and S3D). This strongly suggested that the high TBO uptake of *tpst* seedlings is due to a deficient TPST function in mature endosperm to promote cuticle formation. Notwithstanding, WT endo− seedlings that had received a *tpst* endosperm graft had lower TBO uptake than ungrafted WT endo− seedlings (Figures 3D and S3D). Furthermore, endo+ *tpst* seedlings had lower TBO uptake than endo− *tpst* seedlings (Figure S3A). Hence, these results strongly suggest that TPST is not the only factor promoting seedling cuticle formation in the mature endosperm.

Endospermic PSY1 and CIF2 promote endo– seedling cuticle formation

To identify sulfated peptides involved in seedling cuticle formation, we examined the expression of known genes encoding sulfated peptides upon seed imbibition (Doll et al., 2020; Kaufmann and Sauter, 2019) (STAR Methods). *RGF7*, *PSK1*, *PSK3*, *PSK4, CIF2*, *PSY1*, and *PSY3* have the highest expression (Table S1). Public databases document that *RGF7*, *CIF2*, *PSY1*, and *PSY3* expression is strongly enriched in the endosperm prior and after endosperm rupture (Table S1) (Dekkers et al., 2013). We obtained T-DNA insertion mutant lines for each gene, except *PSK4*, for further study. A standard TBO uptake protocol did not reveal obvious TBO uptake defects in any mutant line. By increasing the duration or temperature of TBO incubation, we detected higher TBO uptake in the cotyledons of *psy1-1* (referred to as *psy1*), *psy1-2* (bearing a promoter insertion strongly diminishing *PSY1* expression), *cif2-2* (referred to as *cif2*), and *cif2-3* endo+ seedlings (Figures 3E, S3E, S4A, S4C, and S4D) (STAR Methods). *cif1/2* double mutants, lacking CIF2 and CIF1, a peptide homologous to CIF2, were similarly, more permeable to TBO than *cif2* seedlings and were also further used in this study (Figures 3E, S3E, and S4A) (STAR Methods). *cif1/2* exhibited hypersensitive arrest responses to ABA, further suggesting the occurrence of cuticle defects (Figure S3B). As mentioned earlier, TEM analysis did not reveal a specific structural defect in the *psy1* or *cif1/2* cuticle but rather a lower contribution of the "thin interface" category and higher contribution of the "thick interface" and "diffuse" categories relative to WT cotyledons (Figure 3F). Strikingly, in the *cif1 cif2 psy1* triple mutant (referred as *cif1/2 psy1*), the contribution of the "thin interface" and "diffuse" categories markedly decreased and increased, respectively (Figure 3G). However, this was not associated with increased TBO uptake in *cif1/2 psy1* mutants relative to *psy1* or *cif1/2* mutants (Figures 3H and S4B). The biophysical alterations leading to higher TBO uptake in a defective cuticle are unknown and may be insufficiently perturbed in *cif1/2 psy1* triple mutants. Altogether, these data confirm the occurrence of seedling cuticle defects in the absence of PSY1 and CIF2. The exacerbated cuticular structural defects observed in TEM with *cif1/2 psy1* triple mutants suggest that PSY1 and CIF2 signal independently to promote seedling cuticle formation.

psy1, *psy1-2*, and *cif1/2* mature endosperm grafted onto WT endo− embryos was less effective than WT endosperm to promote low TBO uptake in WT endo− seedlings (Figures 3I, S4E, and S5A). In contrast, grafting WT mature endosperm could, similarly, promote low TBO uptake to WT, *psy1*, *psy1*-2, and *cif1/2* endo− seedlings (Figures 3J, S4F, and S5B). These results further support the notion that sulfated peptides are required in the endosperm for seedling cuticle formation. The mature endosperm could release PSY1 and CIF2 peptides toward the embryo to promote seedling cuticle formation, or PSY1 and CIF2 could signal within the endosperm to regulate the release of compounds promoting seedling cuticle formation.

Synthetic sulfated CIF2 peptide applied to WT endo− embryos lowered TBO uptake of endo− seedlings, unlike unsulfated CIF2 peptide (Figures 4A and S6A). Yet, TBO uptake of sulfated CIF2-treated endo− seedlings remained higher than that of endo+ seedlings, suggesting that CIF2 is not sufficient to fully promote seedling cuticle formation. Nevertheless, these experiments suggest that the endosperm could release CIF2 to promote seedling cuticle formation without ruling out that CIF2 could also signal within the mature endosperm to enhance its seedling cuticle formation activity. CIF2 signals through GSO1 and GSO2 leucine-rich repeat receptor-like kinases (LRR-RLKs) and notably through GSO1 for Casparian strip formation (Doblas et al., 2017; Nakayama et al., 2017). GSO1 and GSO2 promote embryo development, particularly its epidermis development, and *gso1gso2* seedlings have high TBO uptake (Tsuwamoto et al., 2008). Therefore, we propose that CIF2 signals through GSO1 and GSO2 to promote seedling cuticle formation. The aberrant *gso1gso2* seed shape and mature embryo morphological abnormalities precluded grafting experiments to further test this model (Tsuwamoto et al., 2008).

PSY1 signals through the LRR-RLK PSY1 RECEPTOR (PSY1R) and we obtained two independent *psy1r* insertion lines: *psy1r*, first described by Amano et al., and *psy1r-2* (Amano et al., 2007) (STAR Methods). Cotyledons of *psy1r* and *psy1r-2* endo+ seedlings had high TBO uptake relative to WT endo+ seedlings,

(D) TBO uptake in WT endo− seedlings after grafting WT (1) or *tpst* (2) endosperm onto WT endo− embryos. Statistics as in Figure 2B (n = 18–40).
(E) TBO uptake in WT, *cif1cif2* (*cif1/2*), and *psy1* endo+ seedlings. Statistics as in Figure 3A (n = 40–46).
(F) Cuticle categories contributions (%) in WT, *cif1cif2* (*cif1/2*), and *psy1* endo+ cotyledons. Statistics as in Figure 1C (three biological replicates, n = 104–189).
(G) Cuticle categories contributions (%) in WT and *cif1cif2psy1* (*cif1/2psy1*) endo+ cotyledons. Statistics as in Figure 1E (three biological replicates, n = 177–180).
(H) TBO uptake in WT and *cif1cif2psy1* (*cif1/2psy1*) endo+ seedlings. Statistics as in Figure 3A (n = 20).
(I) Same as Figure 3D using *cif1cif2* or *psy1* mutant seeds. Statistics as in Figure 2B (n = 26–40).
(J) Same as Figure 3C using *cif1cif2* or *psy1* mutant seeds. Statistics as in Figure 2B (n = 38–40).

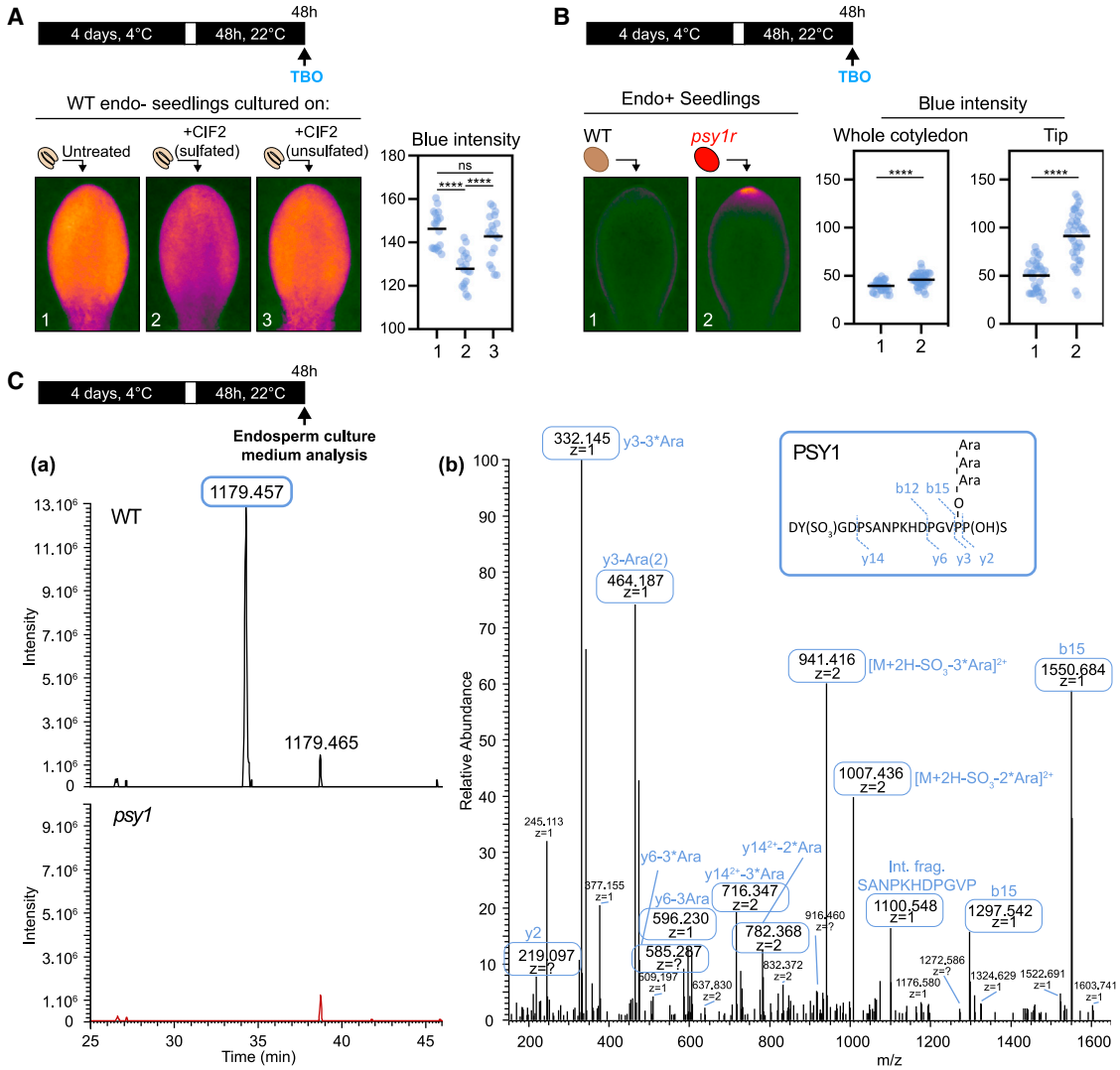

Figure 4. Endospermic PSY1 and CIF2 promote endo– seedling cuticle formation

(A) TBO uptake in WT endo– seedlings after culturing endo– embryos in absence (1) or presence of 1 μM of synthetic sulfated (2) or unsulfated (3) CIF2 peptide. Statistics as in Figure 2B (n = 18).

(B) TBO uptake in WT and *psy1r* endo+ seedlings. Statistics as in Figure 3A (n = 32–38).

(C) Left panel: extracted ion chromatograms in WT and *psy1-1* (*psy1*) endosperm culture mediums of *m/z* 1,179.958 corresponding to a sulfated PSY1 bearing a tri-L-arabinosylated hydroxyproline. Right panel: annotated MS/MS spectrum of the identified sulfated (tri)-arabinosylated PSY1.

particularly at the tips (Figures 4B and S6B). We compared the polyester content between WT and *psy1r* endo+ seedlings. In WT endo+ seedlings, C18:2 DCA was the most abundant oxygenated monomer of cutin, consistent with what is observed in WT endo+ cotyledons (Figure S6C). C18:2 DCA was significantly increased by 1.4-fold in *psy1r* endo+ seedlings. Furthermore, *psy1r* endo+ seedlings also had a significant 1.3-fold increase in ω-hydroxy C18:3 acid (C18:3 ωOH) and about a 1.3-fold increase in overall oxygenated polyester monomers. Increased levels in C18:2 DCA, C18:3 ωOH and overall oxygenated polyester monomers were also observed in WT endo– cotyledons relative to WT endo+ cotyledons, although the increase was more pronounced for C18:2 DCA (3.3-fold) and overall oxygenated polyester monomers (2-fold) (Figure S6C). Overall, these data support the notion that PSY1R-mediated signaling participates to the seedling cuticle formation program promoted by the mature endosperm.

WT endosperm grafts were less effective to lower TBO uptake of *psy1r* endo– cotyledon tips than those of WT endo– cotyledons (Figure S6D). In contrast, WT and *psy1r* endosperm grafts could similarly, lower TBO uptake of WT endo– seedlings (Figure S6E). Thus, PSY1R-mediated signaling is dispensable in the endosperm to promote cuticle formation, indicating that PSY1 promotes cuticle formation by means of its release by the endosperm and perception by PSY1R in the embryo. However, we found that sulfated synthetic PSY1 did not lower TBO uptake of endo– seedlings. This could reflect that the synthetic sulfated PSY1 peptide used lacks a triple L-arabinosylation in a

hydroxyproline present in PSY1, which is important for the biological activity of peptides (Kassaw et al., 2017; Ohyama et al., 2009; Okamoto et al., 2013; Shinohara and Matsubayashi, 2013). Alternatively, synthetic PSY1 may require additional endospermic activities in order to promote seedling cuticle formation.

To directly assess whether the endosperm releases sulfated peptides, we cultured a monolayer of dissected WT, *psy1-1* and *cif2* mature endosperms for 48 h in presence of a thin layer of water (STAR Methods). We could unambiguously detect PSY1 by LC-MS/MS in the WT culture medium but not in the *psy1* medium (Figure 4C). The observed PSY1 mass corresponded to a sulfated PSY1 bearing a tri-L-arabinosylated hydroxyproline, confirming that PSY1 is also subject to sulfation and L-arabinolysation in the seed mature endosperm (Figure 4C). We did not detect CIF1 or CIF2 peptides, indicating that in these samples, CIF1 and CIF2 were below the limit of detection of the mass spectrometry instrument. Overall, the data are consistent with the model that the release of sulfated peptides promotes seedling cuticle formation.

Next, we studied the developmental defects of endo− seedlings.

The endosperm is necessary for normal photomorphogenic and skotomorphogenic development

In the presence of light, the cotyledon surface and root length of endo− seedlings were reduced, true leaf emergence was delayed, and only about 25% of endo− seedlings were able to survive (Figures 5A and S7A). In the absence of light, endo− seedlings lost their apical hook and opened their cotyledons as early as 2 days after stratification, unlike endo+ seedlings, and had shorter hypocotyl and root length (Figures 5B and S7B; Video S1).

As mentioned earlier, endosperm removal compromised seedling development only when removed prior to germination (Figure S7C). Grafting WT endosperm onto WT embryos did not restore normal photomorphogenesis or skotomorphogenesis in endo− seedlings. In contrast, WT embryos cultured on a bed of WT endosperm/seed coat tissues produced endo− seedlings whose development was markedly improved even when a nylon mesh separated embryos and endosperm/seed coat tissues (Figures 5A, 5B, and S7D) (Lee et al., 2010). Furthermore, the rescue was observed when using only endosperm tissue but not when using only seed coat (testa) tissue (Figure S7E). Altogether, these observations strongly indicate that the endosperm releases diffusible activities necessary for normal seedling establishment.

Developmental defects of endosperm-less embryos likely do not arise from limiting carbon supplies

The endosperm contains 10% of triacylglycerols (TAGs) stored in seeds (Penfield et al., 2004). We investigated the role of endospermic TAG stores in seedling development.

PEROXISOMAL ABC TRANSPORTER1 (*PXA1*) encodes a peroxisomal ATP-binding cassette (ABC) transporter essential for acyl CoAs import into the peroxisome and TAGs breakdown (Footitt et al., 2002). SCBAs using WT and *pxa1-1* (*pxa1*) endosperms with WT embryos similarly rescued the developmental defects of WT endo− seedlings (Figure S7F). Seeds exposed to ABA fail to germinate and block TAG catabolism in the embryo but not in the endosperm (Penfield et al., 2006). After exposing WT seeds to ABA for 8 days, which depletes 95% of TAG content in the endosperm, ungerminated seeds were transferred to a normal medium and their endosperm was either removed or not. Endo+ embryos produced normal seedlings, unlike endo− embryos (Figure S7G). Endo− seedling developmental defects could be due to a defective TAG catabolism in endo− embryos. However, levels of the 20:1 TAG, a marker for mature seed lipid stores, declined at similar rates in endo− and endo+ embryos upon imbibition in both the presence and absence of light (Figure S7H).

Endo− seedling health was marginally improved by exogenous sucrose, which improved root growth but did not rescue cotyledon growth and seedling development (Figure S7I). The effect of sucrose on root growth is not surprising, given the known stimulatory effect of sucrose on root growth (Macgregor et al., 2008; Wu et al., 2005). Altogether, these experiments indicate that removal of endospermic TAGs in endo− embryos does not readily explain the developmental defects of endo− seedlings.

The abnormal endo– seedling transcriptome is largely restored by a SCBA

In the presence of light, the expression of 2,994 and 1,851 genes was down-regulated and up-regulated, respectively, in WT endo− seedlings relative to endo+ seedlings (Figure 5C). Strikingly, in WT endo− seedlings arising from a SCBA using WT endosperms/seed coats, as much as 95% of genes had their expression either fully or partially restored (Figure 5C). Similarly, in darkness, the SCBA partially or fully restored the expression of 70% of genes deregulated in endo− seedlings (Figure 5C). Unsurprisingly, numerous genes involved in cuticle formation were mis-regulated in endo− seedlings, and their expression was restored in endo− seedlings arising from a SCBA (Figure 5D). This included the misregulation of wax biosynthesis genes, such as *CER1*, *CER8*, *CER3/WAX2*, and several *KCSs*, which are regarded as crucial for sealing the cuticle (Schreiber and Schönherr, 2009). However, misexpression of cuticle formation genes did not readily account for the polyester composition defects of WT endo− seedlings. For example, expression of *CYP86A4*, encoding a fatty acid ω-hydroxylase, was reduced in endo− seedlings, whereas their oxygenated fatty acid content was increased (Figures 5D and 1F). Hence, the cuticle defects in WT endo− seedlings likely also reflect deregulated enzymatic activities for cuticle formation.

A gene ontology (GO) enrichment analysis revealed that in the presence of light, down-regulated genes in endo− seedlings relative to endo+ seedlings are associated with cell wall (suberin biosynthetic processes, plant-type cell wall loosening, plant-type secondary cell wall biogenesis, pectin catabolic processes), and metabolic processes (glucosinolate biosynthetic processes, nucleotide-sugar biosynthetic processes) (Table S2). Up-regulated genes in endo− seedlings are associated with response to stimuli (cellular response to hypoxia, response to chitin, response to salicylic acid). In darkness, down-regulated genes in endo− seedlings are associated with light signaling (response to absence of light, response to red or far red light), regulation of seed germination, and response to phytohormones

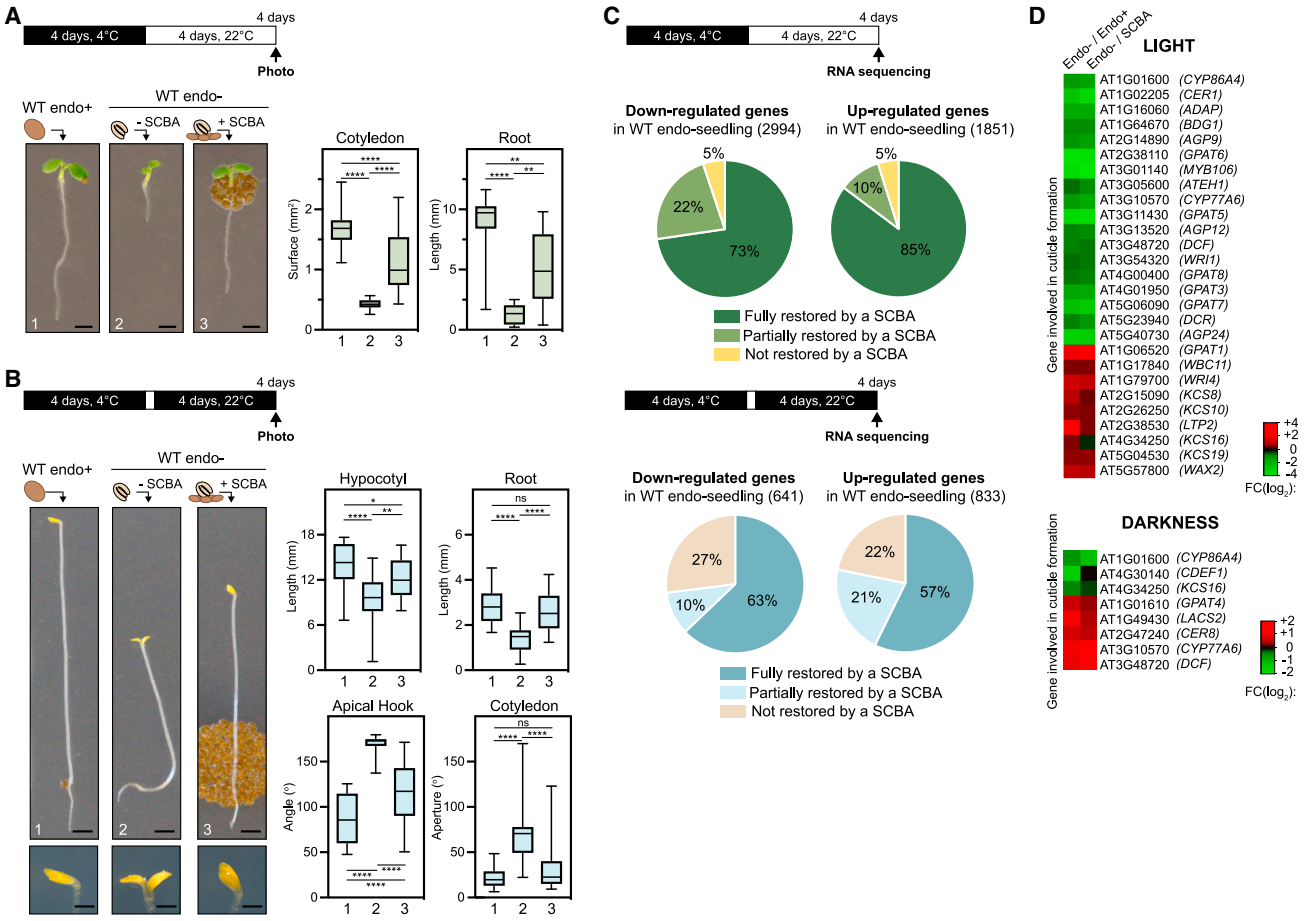

Figure 5. The endosperm is necessary for normal photomorphogenic and skotomorphogenic development

(A) Representative pictures of WT endo+ seedlings (1), WT endo− seedlings non-exposed (2) or exposed (3) to a SCBA 4 days after stratification with light (bars, 1 mm). Boxplots provide quantification of cotyledons surface and root length. Data represent the median ± min to max (two biological replicates, n = 22–40). Statistical differences as assessed by one-way ANOVA test followed by a post-hoc Tukey test.

(B) Same as A except that plant material was maintained in darkness after stratification (bars, 0.4 mm). Closeup images of cotyledons and apical hypocotyl regions are shown (bars, 1 mm). Boxplots provide quantification data of hypocotyl length, root length, apical hook development, by measuring the angle between the hypocotyl axes and cotyledons, and cotyledon aperture. Statistics as in Figure 5A (four biological replicates, n = 25–26).

(C) Pie chart representing the distribution of different categories of the genes mis-regulated in endo− seedlings. The differentially expressed genes between endo− seedlings and endo+ seedlings were selected according to the value threshold (fold change ≥ 1.5 or ≤ 0.67) after significance analysis and false discovery rate (FDR < 0.05) analysis. The genes fully or partially restored by SCBA were defined according to the value threshold (fold change ≥ 1.3 or ≤ 0.77) comparing endo− seedling with SCBA. The genes fully restored by the SCBA were defined according to the value threshold (fold change ≥ 0.8 and ≤ 1.25) comparing SCBA with endo+ seedling.

(D) Heatmap representing the expression of genes involving cuticle formation, which were mis-regulated in endo− seedlings, identified in the RNA-seq experiments in dark (bottom) and light conditions (top). The red and green horizontal bars represent the relative expression levels in endo− seedlings compared with those in endo+ seedling and endo− seedlings arising from a SCBA.

(response to ethylene, response to auxin), whereas up-regulated genes are related to the synthesis and regulation of the photosynthetic machinery and photosynthesis (photosynthetic electron transport in photosystem I, chlorophyll biosynthetic processes, and regulation of photosynthesis) (Table S2). Given its importance, we characterized further chloroplast function in endo− seedlings in the absence or presence of light.

Endo- seedlings have abnormal chloroplast function

WT endo− seedlings cultivated in the dark for 4 days and transferred to light failed to green and bleached, unlike endo+ seedlings (Figure 6A). Photobleaching may reflect excessive accumulation of protochlorophyllide (PChlide), a tightly regulated precursor of chlorophyll that can provoke photooxidative damage upon transfer to light (Meskauskiene et al., 2001). Indeed, endo− seedlings cultivated in darkness had higher PChlide fluorescence levels relative to endo+ seedlings (Figures 6B and S8A) (Pineau et al., 1986). Strikingly, a SCBA lowered PChlide fluorescence emission and photobleaching (Figures 6A, 6B, and S8A).

In the presence of light, WT endo− seedlings had a pale-green appearance, suggesting an impairment in chloroplast development. Accordingly, the quantum yield of photosystem II (ΦPSII) under light was low in endo− seedlings (Figure 6C). In contrast, endo− seedlings arising from a SCBA had a ΦPSII similar to that

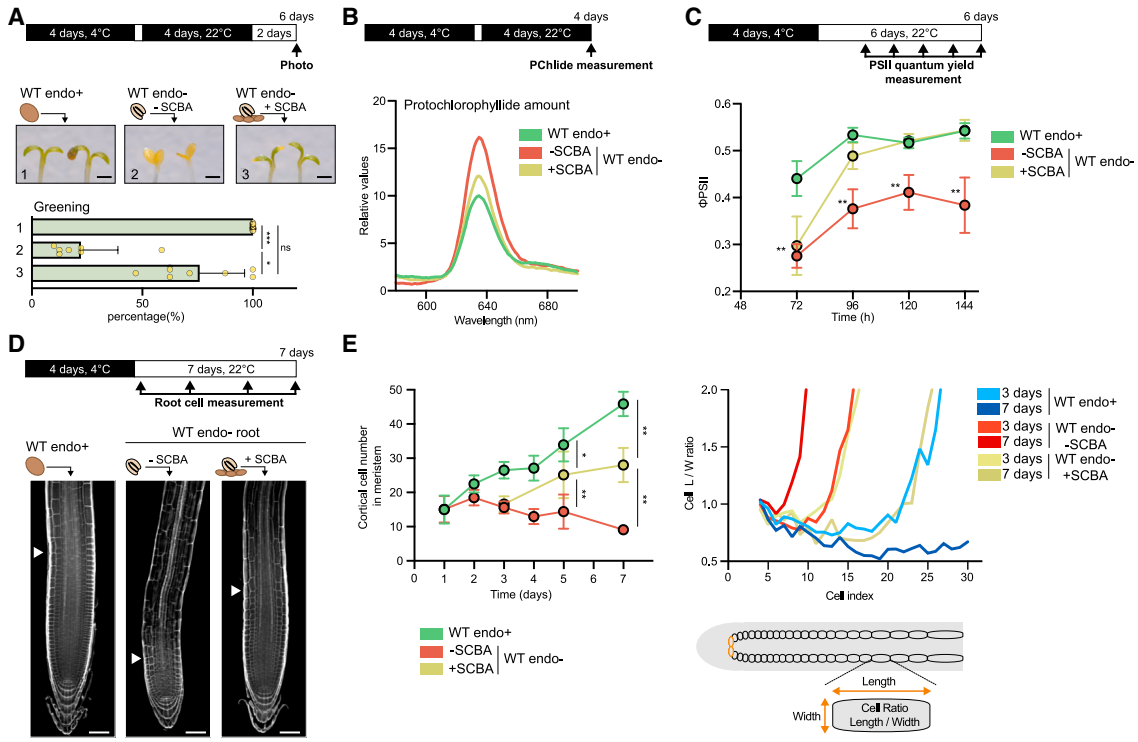

Figure 6. The endosperm is necessary for chloroplast function and primary root development

(A) Representative pictures of WT endo+ seedlings (1), WT endo− seedlings non-exposed (2) or exposed (3) to a SCBA for 2 days with light after 4 days without light (bars, 0.5 mm). Histogram shows survival percentage. Statistics as in Figure 1C (seven biological replicates, n = 7).

(B) Fluorescence profile of extracts from etiolated seedlings excited at 440 nm, expressed in relative fluorescence units.

(C) Quantum yield of Photosystem II (ΦPSII) at 180 μmol photons m^{-2} s^{-1} of PAR light. Data represent the mean ± SD (two biological replicates, n = 6). Statistical differences as assessed by Kruskal-Wallis test followed by a pairwise Mann-Whitney test for multiple comparisons.

(D) Representative images of roots of WT endo+ seedlings (1), WT endo− seedlings non-exposed (2) or exposed (3) to a SCBA 4 days after stratification (bars, 50 μm). Arrowhead indicates the end of the meristematic zone.

(E) Left panel: meristem zone cortical cell number of WT endo+ and endo− seedlings roots over time after stratification. Values for WT endo− seedlings exposed to a SCBA are shown at 3, 5, and 7 days. Data represent the mean ± SD Statistics as Figure 6C (n = 3–20). Right panel: cortical cell length to width ratio in WT endo+ seedlings and endo− seedlings cultured in absence or presence of a SCBA.

of endo+ seedlings (Figure 6C). However, the maximum quantum yield of PSII (Fv/Fm) differed only in the earlier time point (72 h after light exposure), and the difference between endo− seedlings arising from a SCBA and endo+ seedlings disappeared in later time points (Figure S8B). The lower ΦPSII correlated with an increase in thermal dissipation (NPQ), and a higher fraction of open PSII reaction centers, as estimated by the qL parameter, in the earlier time points (Figure S8B) (Kramer et al., 2004). These results show that the endosperm is essential for normal plastid development in seedlings.

Endo- seedlings have abnormal primary root development

The *Arabidopsis* root is organized in concentric, cylindrically shaped, single-cell layers of distinct cell types that include epidermal, cortical, endodermal, and pericyclic cells (Petricka et al., 2012). All root cells are continuously produced by dividing stem cells surrounding a "quiescent center" in the root apical meristem (RAM). Dividing cells define the meristematic zone, which is followed, shootward, by transition, elongation, and differentiation zones. In WT endo+ seedlings, the meristematic zone increased from 16 to 35 cells during the first 7 days after stratification, consistent with previous reports (Figures 6D and 6E) (González-García et al., 2011). During the same period, the meristematic zone of WT endo− seedlings went from 16 cells to about 10 cells (Figures 6D and 6E). A SCBA using WT endosperms and WT embryos corrected the size of the meristematic zone as early as 5 days upon stratification (Figure 6D). Altogether, these observations show that the endosperm is essential for normal root meristem development.

DISCUSSION

The seedling cuticle is formed during the embryo-to-seedling transition

A well-sealed cuticle conferring low TBO uptake and a tannic cell wall of maternal origin cover the outer surface of the mature endosperm and protect the seed's living tissues (De Giorgi et al., 2015; Demonsais et al., 2020; Loubéry et al., 2018) (Figure 7). We speculate that these protective structures may enable the mature embryo to afford a more permeable and less protective cuticle that enables endospermic ABA uptake for the control

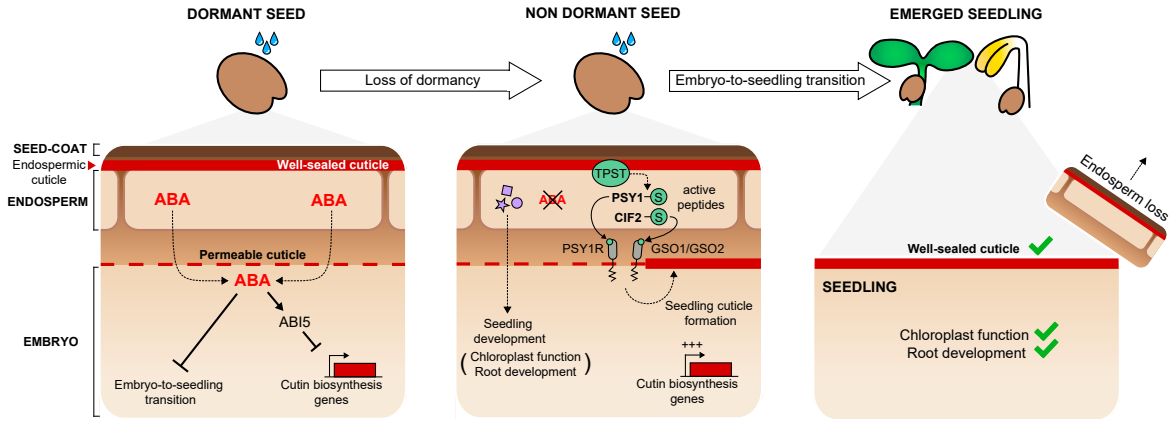

Figure 7. Model describing control of germination and seedling development by the mature endosperm

In dormant seeds (left panel) endospermic ABA represses germination and expression of cutin biosynthetic genes through the TF ABI5. In non-dormant seeds (middle panel), ABA synthesis ceases, and unknown endospermic activities, represented by a star, circle, and square symbol, are released toward the embryo to promote seedling development. Release of tyrosyl sulfate transferase (TPST)-sulfated CIF2 and PSY1 peptides from the endosperm promotes seedling cuticle development by activating PSY1R and GSO1/2 receptors.

of seed germination. Indeed, here, we found that the embryonic cuticle has high TBO uptake relative to the seedling cuticle and a different structural organization, as observed by TEM (Figures 1A and 1C). Interestingly, when seeds block their germination, endogenous ABA accumulation increases and represses the expression of cutin biosynthesis genes (De Giorgi et al., 2015; Lee et al., 2010, 2012) (Figure 7). In contrast, seeds committed to germinate strongly induce the expression of cutin biosynthesis genes prior to seed germination (De Giorgi et al., 2015). This is consistent with the rapid formation of a well-sealed seedling cuticle, characterized by its lower TBO uptake and distinct cuticle structural organization, during the embryo-to-seedling transition. Hence, the seedling cuticle is strongly fortified during the embryo-to-seedling transition (Figure 7). Mutants defective in cuticle formation display hypersensitive growth arrest response to ABA after germination (Figure 2D). This supports the speculation that a well-sealed cuticle in mature embryos would not be compatible with the control of seed germination through the release of ABA by the endosperm.

The mature endosperm governs seedling cuticle formation through peptide signalization

Surprisingly, seedling cuticle formation is controlled by the mature endosperm, as shown by grafting experiments (Figures 2B and 2C). Thus, when the seed is committed to germinate, the endosperm stops releasing ABA and promotes seedling cuticle formation (Figure 7). Our data suggest a model where PSY1 and CIF2 are activated by TPST in the endosperm and then released toward the embryo. In the embryo, PSY1 is perceived by PSY1R, whereas CIF2 is perceived by GSO1 and GSO2 to promote cuticle formation (Figure 7). This unidirectional regulation system is similar to that found in roots where sulfonated CIF1 and CIF2 peptides are released from the stele to promote Casparian strip formation via SNG3/GSO2 signaling (Doblas et al., 2017; Pfister et al., 2014). Interestingly, *psy1r* mutant's high uptake of TBO occurs mostly at the cotyledon tip region whereas *psy1* mutant's uptake of TBO is more homogeneous throughout the cotyledon's surface (Figures 3E and 4B). This could reflect compensatory effects mediated by PSY2 or PSY3, which also signal through PSY1R (Kaufmann and Sauter, 2019). Alternatively, absence of PSY1 in *psy1* mutants could modify TPST sulfation activity toward other sulfated peptides, which could modify their activity to promote cuticle formation in a manner that is different from that in *psy1r* mutants where PSY1R signaling is abolished but PSY1 continues to accumulate. We found that the endosperm can promote cuticle formation in a TPST-independent manner. Indeed, *tpst* endo− seedlings had higher TBO uptake than *tpst* endo+ seedlings, and grafted *tpst* endosperm retained some capability to lower TBO uptake in WT endo− seedlings (Figures S3A and S3D). TPST-mediated sulfated peptide signaling in the context of seedling cuticle formation remains to be fully understood. If sulfated peptides substantially rely on sulfation to bind to their receptors and if sulfation is only carried by TPST, then *tpst* mutants ought to have similar phenotypes, if not stronger, than those observed with individual peptide mutants or with mutants lacking the sulfated peptide receptors. This is clearly not the case for sulfated peptide signaling through GSO1 and GSO2 receptors. Indeed, although TBO uptake phenotypes of *tpst* seedlings are indeed stronger than those of *cif2* mutants, they are mild when compared with those of *gso1gso2* seedlings (Doll et al., 2020; Tsuwamoto et al., 2008). This indicates that GSO1 and GSO2 are able to signal even in the absence of TPST, suggesting that another sulfation activity is present in *tpst* cells or that GSO receptors can still signal in response to nonsulfated peptides or that GSO receptors can signal in response to other ligands. The strong TBO uptake of *gso1gso2* seedlings could also reflect a different cell wall or intracellular composition, which retains more TBO, thus increasing tissue coloration.

The seedling cuticle is likely formed by reorganizing the embryonic cuticle, which arises during the globular stage (Szczuka and Szczuka, 2003). A recent report proposed that the globular embryo autonomously produces discontinuous cuticle stretches, leaving gaps. A gap-filling bidirectional

signaling model involving the globular embryo and the developing endosperm was proposed: a TWS1 peptide sulfated by TPST is generated and released by the embryo toward the endosperm where it is activated by the subtilisin-peptidase ALE1 and sent back to the embryo where it signals through the GSO1/GSO2 receptors (Doll et al., 2020). Together with our findings, this would suggest that the endosperm influences cuticle formation throughout seed development all the way to seedling establishment by means of specific sulfate peptide signaling mechanisms adapted to the particular ongoing developmental stage. It might be noteworthy that the bidirectional signaling model involving the globular embryo and endosperm was based, in part, on TBO uptake phenotypes observed in seedlings, i.e., in mutant seedlings or in mutant seedlings complemented with transgenic promoters conferring globular embryo- and endosperm-enriched expression during embryogenesis (Doll et al., 2020). Given that the seedling acquires its low TBO uptake property only after germination, it is unclear whether the observed low or high TBO uptake phenotypes reflect the activity of the gene products during the embryo globular stage or their particular activity in the embryo, the endosperm or both during seed development after the globular stage or during the embryo-to-seedling transition.

The endosperm governs other essential aspects of seedling development

Intriguingly, we found that viable seedling formation also requires endospermic diffusible activities. The developmental defects in endo− seedlings were not straightforwardly attributable to limiting food supplies (Figures S7F–S7I). The endosperm and seed coat shield the embryo from an oxidative environment, so that the developmental defects of endo− seedlings may reflect oxidative damage. Against this possibility, endo− embryos cultured on a bed of endosperms are exposed to an oxidative environment just as control endo− embryos (e.g., Figures S7D or S7E); yet, the endo− seedlings defects are only corrected when endo− embryos are exposed to the endosperms. Mutants with cuticular defects, such as *bdg*, *lacs2*, or *gpat4gpat8* mutants, are able to produce viable seedlings and endosperm grafts promote seedling cuticle formation in endo− seedlings without correcting their other developmental defects. Hence, it is unlikely that the entire set of endo− seedlings developmental defects simply reflect their deficient cuticle. Besides photosynthesis, chloroplast function influences, directly or indirectly, numerous, if not all, cellular and plant developmental processes, including those pertaining to hormone synthesis (Chan et al., 2016). Hence, a defective chloroplast could be a major cause for the developmental defects in endo− seedlings. Understanding endospermic function to promote seedling development will require a full description of the endosperm secretome.

The "how" and "why" of the endosperm's role in seedling development remain largely unknown

The evolutionary origin of the endosperm is enigmatic, and it remains to be understood why in *Arabidopsis* the embryo relies so heavily on the endosperm for viable seedling establishment. The success of angiosperms lies notably on successful seed dispersal but also in the capacity to control seed germination according to seasonal or environmental cues. The making of a highly resistant and mobile embryo implies introducing extreme cellular and developmental adaptations, such as desiccation and a small size. This potentially poses a dilemma, since the more extreme adaptation schemes may conflict with the capacity to control germination or produce a viable seedling. An "altruist" peripheral tissue, such as the endosperm, with lower survival and developmental expectations, could represent a means to address this dilemma. Hence, the *Arabidopsis* mature endosperm would sense environmental cues to control germination, through the release of ABA, and provide developmental activities aiding the embryo to successfully form a seedling from a highly resistant embryo. Interestingly, ABA represses lipid catabolism in the embryo but not in the endosperm (Penfield et al., 2006). This supports the speculation that the endosperm is a proactive tissue relative to the embryo.

Limitations of the study

In this study, we showed that TPST activity in the endosperm promotes seedling cuticle formation, involving TPST-mediated sulfation of PSY1 and CIF2. However, our data indicate that other endosperm sulfated peptides are likely involved since the TBO uptake phenotypes of *psy1*, *cif2*, and *psy1/cif1/cif2* mutants are weaker than those of the *tpst* mutant. In addition, our data indicate that TPST is not the only endosperm factor promoting cuticle formation since endosperm removal of *tpst* seeds further increases TBO uptake in *tpst* seedlings. This suggests that other unidentified endosperm activities, unrelated to TPST and sulfated peptide signaling, promote seedling cuticle formation.

The grafting procedure introduced here requires that the anatomy of the mutant seeds used to dissect the endosperm and embryo does not deviate substantially from the WT anatomy so as to ensure close fitting when grafting the endosperm onto the embryo. In mutant seeds with severe anatomical defects, such as the *gso1/gso2* mutants, dissecting intact endosperm and embryo tissues suitable for grafting can be very difficult, which makes the technique unpractical and unreliable.

STAR★METHODS

Detailed methods are provided in the online version of this paper and include the following:

- KEY RESOURCES TABLE
- RESOURCE AVAILABILITY
  - Lead contact
  - Materials availability
  - Data and code availability
- EXPERIMENTAL MODEL AND SUBJECT DETAILS
  - Plant material and growth conditions
- METHODS DETAILS
  - Seed germination and seedling growth assays
  - Dissection and grafting procedures
  - TBO uptake assays
  - RT-qPCR
  - RNAseq
  - Gene expression profile
  - Transmission electron microscopy
  - Digital warping and TBO staining quantification procedures

- Root development analysis
- Cutin analysis
- Sample preparation for mass spectrometry
- Mass spectrometry analyses
- Leakage control
- Fatty acid methyl esters (FAME) preparation and analysis
- Fluorescence Analysis

- QUANTIFICATION AND STATISTICAL ANALYSIS

SUPPLEMENTAL INFORMATION

Supplemental information can be found online at https://doi.org/10.1016/j.devcel.2021.10.005.

ACKNOWLEDGMENTS

We thank Anja Thoe Fuglsang for providing *psy1-1* and *psy1r-1* seed material, Niko Geldner for providing *tpst-1*, *sgn2-1*, and *cif1cif2* seeds, and Steven Penfield for providing *pxa1-1* seeds. We thank Christian Megies and Yashar Sadian for technical assistance. We thank Miguel Moreno-Risueño and Marie Barberon for helpful discussions. This work was supported by the Swiss National Science Foundation grants to L.L.-M. (grant nos. 31003A-152660/1 and 31003A-179472/1) and the State of Geneva, Switzerland.

AUTHOR CONTRIBUTIONS

L.L.-M. conceived, supervised, and raised funding for the project; J.D.G., M.I., S.L., and L.L.-M. designed the experiments; J.D.G. performed most of the experiments; M.I. analyzed transcriptome sequencing data; S.L. supervised imaging experiments and wrote code for imaging analysis; P.W. performed LC-MS/MS experiments; L.M.-S. performed fatty acid methyl esters (FAME) experiments; K.G. and C.N. performed polyester measurement experiments; F.P.L. performed photosynthesis experiments; S.F. generated the *cif2-3* mutant line; C.F., W.K., A.U.-P., U.P., and S.L. provided technical assistance; L.L.-M. wrote original draft; C.N., M.I., and L.L-M. wrote, reviewed, and edited manuscript, and all authors commented on the manuscript.

DECLARATION OF INTERESTS

The authors declare no competing interests.

INCLUSION AND DIVERSITY

One or more of the authors of this paper self-identifies as a member of the LGBTQ+ community.

Received: March 19, 2021
Revised: August 19, 2021
Accepted: October 5, 2021
Published: October 26, 2021

REFERENCES

Ali-Rachedi, S., Bouinot, D., Wagner, M.H., Bonnet, M., Sotta, B., Grappin, P., and Jullien, M. (2004). Changes in endogenous abscisic acid levels during dormancy release and maintenance of mature seeds: studies with the Cape Verde Islands ecotype, the dormant model of Arabidopsis thaliana. Planta *219*, 479–488.

Amano, Y., Tsubouchi, H., Shinohara, H., Ogawa, M., and Matsubayashi, Y. (2007). Tyrosine-sulfated glycopeptide involved in cellular proliferation and expansion in Arabidopsis. Proc. Natl. Acad. Sci. USA *104*, 18333–18338.

Baroux, C., and Grossniklaus, U. (2019). Seeds-An evolutionary innovation underlying reproductive success in flowering plants. Curr. Top. Dev. Biol. *131*, 605–642.

Baroux, C., Spillane, C., and Grossniklaus, U. (2002). Evolutionary origins of the endosperm in flowering plants. Genome Biol. *3*, reviews1026.

Berhin, A., de Bellis, D., Franke, R.B., Buono, R.A., Nowack, M.K., and Nawrath, C. (2019). The root cap cuticle: a cell wall structure for seedling establishment and lateral root formation. Cell *176*, 1367–1378.e8.

Bessire, M., Chassot, C., Jacquat, A.C., Humphry, M., Borel, S., Petétot, J.M., Métraux, J.P., and Nawrath, C. (2007). A permeable cuticle in Arabidopsis leads to a strong resistance to Botrytis cinerea. EMBO J *26*, 2158–2168.

Bethke, P.C., Libourel, I.G., Aoyama, N., Chung, Y.Y., Still, D.W., and Jones, R.L. (2007). The Arabidopsis aleurone layer responds to nitric oxide, gibberellin, and abscisic acid and is sufficient and necessary for seed dormancy. Plant Physiol. *143*, 1173–1188.

Blankenberg, D., Von Kuster, G., Coraor, N., Ananda, G., Lazarus, R., Mangan, M., Nekrutenko, A., and Taylor, J. (2010). Galaxy: a web-based genome analysis tool for experimentalists. Curr. Protoc. Mol. Biol. *89*, 19.10.1–19.10.21.

Bogovic, J.A., Hanslovsky, P., Wong, A., and Saalfeld, S. (2016). Robust registration of calcium images by learned contrast synthesis. In 2016 IEEE 13th International Symposium on Biomedical Imaging (ISBI), pp. 1123–1126.

Bourgault, R., Matschi, S., Vasquez, M., Qiao, P., Sonntag, A., Charlebois, C., Mohammadi, M., Scanlon, M.J., Smith, L.G., and Molina, I. (2020). Constructing functional cuticles: analysis of relationships between cuticle lipid composition, ultrastructure and water barrier function in developing adult maize leaves. Ann. Bot. *125*, 79–91.

Chan, K.X., Phua, S.Y., Crisp, P., McQuinn, R., and Pogson, B.J. (2016). Learning the languages of the chloroplast: retrograde signaling and beyond. Annu. Rev. Plant Biol. *67*, 25–53.

De Giorgi, J., Piskurewicz, U., Loubery, S., Utz-Pugin, A., Bailly, C., Mène-Saffrané, L., and Lopez-Molina, L. (2015). An endosperm-associated cuticle is required for Arabidopsis Seed viability, dormancy and early control of germination. PLoS Genet. *11*, e1005708.

Dekkers, B.J., Pearce, S., van Bolderen-Veldkamp, R.P., Marshall, A., Widera, P., Gilbert, J., Drost, H.G., Bassel, G.W., Müller, K., King, J.R., et al. (2013). Transcriptional dynamics of two seed compartments with opposing roles in Arabidopsis seed germination. Plant Physiol. *163*, 205–215.

Demonsais, L., Utz-Pugin, A., Loubéry, S., and Lopez-Molina, L. (2020). Identification of tannic cell walls at the outer surface of the endosperm upon Arabidopsis seed coat rupture. Plant J. *104*, 567–580.

Doblas, V.G., Smakowska-Luzan, E., Fujita, S., Alassimone, J., Barberon, M., Madalinski, M., Belkhadir, Y., and Geldner, N. (2017). Root diffusion barrier control by a vasculature-derived peptide binding to the SGN3 receptor. Science *355*, 280–284.

Doll, N.M., Royek, S., Fujita, S., Okuda, S., Chamot, S., Stintzi, A., Widiez, T., Hothorn, M., Schaller, A., Geldner, N., and Ingram, G. (2020). A two-way molecular dialogue between embryo and endosperm is required for seed development. Science *367*, 431–435.

Fabre, G., Garroum, I., Mazurek, S., Daraspe, J., Mucciolo, A., Sankar, M., Humbel, B.M., and Nawrath, C. (2016). The ABCG transporter PEC1/ABCG32 is required for the formation of the developing leaf cuticle in Arabidopsis. New Phytol. *209*, 192–201.

Footitt, S., Slocombe, S.P., Larner, V., Kurup, S., Wu, Y., Larson, T., Graham, I., Baker, A., and Holdsworth, M. (2002). Control of germination and lipid mobilization by COMATOSE, the Arabidopsis homologue of human ALDP. EMBO J *21*, 2912–2922.

Giardine, B., Riemer, C., Hardison, R.C., Burhans, R., Elnitski, L., Shah, P., Zhang, Y., Blankenberg, D., Albert, I., Taylor, J., et al. (2005). Galaxy: a platform for interactive large-scale genome analysis. Genome Res. *15*, 1451–1455.

Goecks, J., Nekrutenko, A., and Taylor, J.; Galaxy Team (2010). Galaxy: a comprehensive approach for supporting accessible, reproducible, and transparent computational research in the life sciences. Genome Biol. *11*, R86.

González-García, M.P., Vilarrasa-Blasi, J., Zhiponova, M., Divol, F., Mora-García, S., Russinova, E., and Caño-Delgado, A.I. (2011). Brassinosteroids

control meristem size by promoting cell cycle progression in Arabidopsis roots. Development *138*, 849–859.

Ingram, G., and Nawrath, C. (2017). The roles of the cuticle in plant development: organ adhesions and beyond. J. Exp. Bot. *68*, 5307–5321.

Jakobson, L., Lindgren, L.O., Verdier, G., Laanemets, K., Brosché, M., Beisson, F., and Kollist, H. (2016). BODYGUARD is required for the biosynthesis of cutin in Arabidopsis. New Phytol. *211*, 614–626.

Jarvis, P., and López-Juez, E. (2013). Biogenesis and homeostasis of chloroplasts and other plastids. Nat. Rev. Mol. Cell Biol. *14*, 787–802.

Jeffree, C.E. (2006). The fine structure of the plant cuticle. In Biology of the Plant Cuticle, M. Riederer and C. Müller, eds. (Blackwell Publishing)), pp. 11–125.

Kassaw, T., Nowak, S., Schnabel, E., and Frugoli, J. (2017). ROOT DETERMINED NODULATION1 is required for M. truncatula CLE12, but not CLE13, peptide signaling through the SUNN receptor kinase. Plant Physiol. *174*, 2445–2456.

Kaufmann, C., and Sauter, M. (2019). Sulfated plant peptide hormones. J. Exp. Bot. *70*, 4267–4277.

Kinoshita, N., Berr, A., Belin, C., Chappuis, R., Nishizawa, N.K., and Lopez-Molina, L. (2010). Identification of growth insensitive to ABA3 (gia3), a recessive mutation affecting ABA Signaling for the control of early post-germination growth in *Arabidopsis thaliana*. Plant Cell Physiol, 239–251. https://doi.org/10.1093/pcp/pcp183.

Komori, R., Amano, Y., Ogawa-Ohnishi, M., and Matsubayashi, Y. (2009). Identification of tyrosylprotein sulfotransferase in Arabidopsis. Proc. Natl. Acad. Sci. USA *106*, 15067–15072.

Kramer, D.M., Johnson, G., Kiirats, O., and Edwards, G.E. (2004). New fluorescence parameters for the determination of QA redox state and excitation energy fluxes. Photosynth. Res. *79*, 209.

Kurdyukov, S., Faust, A., Nawrath, C., Bär, S., Voisin, D., Efremova, N., Franke, R., Schreiber, L., Saedler, H., Métraux, J.P., and Yephremov, A. (2006). The epidermis-specific extracellular BODYGUARD controls cuticle development and morphogenesis in Arabidopsis. Plant Cell *18*, 321–339.

Lee, E.J., Kim, K.Y., Zhang, J., Yamaoka, Y., Gao, P., Kim, H., Hwang, J.U., Suh, M.C., Kang, B., and Lee, Y. (2021). Arabidopsis seedling establishment under waterlogging requires ABCG5-mediated formation of a dense cuticle layer. New Phytol. *229*, 156–172.

Lee, K.P., and Lopez-Molina, L. (2013). A seed coat bedding assay to genetically explore in vitro how the endosperm controls seed germination in Arabidopsis thaliana. J. Vis. Exp. *81*, e50732.

Lee, K.P., Piskurewicz, U., Turečková, V., Carat, S., Chappuis, R., Strnad, M., Fankhauser, C., and Lopez-Molina, L. (2012). Spatially and genetically distinct control of seed germination by phytochromes A and B. Genes Dev. *26*, 1984–1996.

Lee, K.P., Piskurewicz, U., Turecková, V., Strnad, M., and Lopez-Molina, L. (2010). A seed coat bedding assay shows that RGL2-dependent release of abscisic acid by the endosperm controls embryo growth in Arabidopsis dormant seeds. Proc. Natl. Acad. Sci. USA *107*, 19108–19113.

Li, Y., Beisson, F., Koo, A.J., Molina, I., Pollard, M., and Ohlrogge, J. (2007). Identification of acyltransferases required for cutin biosynthesis and production of cutin with suberin-like monomers. Proc. Natl. Acad. Sci. USA *104*, 18339–18344.

Li-Beisson, Y., Shorrosh, B., Beisson, F., Andersson, M.X., Arondel, V., Bates, P.D., Baud, S., Bird, D., Debono, A., Durrett, T.P., et al. (2013). Acyl-lipid metabolism. Arabidopsis Book *11*, e0161. https://doi.org/10.1199/tab.0161.

Lopez-Molina, L., Mongrand, S., and Chua, N.H. (2001). A postgermination developmental arrest checkpoint is mediated by abscisic acid and requires the ABI5 transcription factor in Arabidopsis. Proc. Natl. Acad. Sci. USA *98*, 4782–4787.

Lopez-Molina, L., Mongrand, S., McLachlin, D.T., Chait, B.T., and Chua, N.H. (2002). ABI5 acts downstream of ABI3 to execute an ABA-dependent growth arrest during germination. Plant J. *32*, 317–328.

Loubéry, S., De Giorgi, J., Utz-Pugin, A., Demonsais, L., and Lopez-Molina, L. (2018). A maternally deposited endosperm cuticle contributes to the physiological defects of transparent testa seeds. Plant Physiol. *177*, 1218–1233.

Luhua, S., Hegie, A., Suzuki, N., Shulaev, E., Luo, X., Cenariu, D., Ma, V., Kao, S., Lim, J., Gunay, M.B., et al. (2013). Linking genes of unknown function with abiotic stress responses by high-throughput phenotype screening. Physiol. Plant. *148*, 322–333.

Macgregor, D.R., Deak, K.I., Ingram, P.A., and Malamy, J.E. (2008). Root system architecture in Arabidopsis grown in culture is regulated by sucrose uptake in the aerial tissues. Plant Cell *20*, 2643–2660.

Maxwell, K., and Johnson, G.N. (2000). Chlorophyll fluorescence–a practical guide. J. Exp. Bot. *51*, 659–668.

Meskauskiene, R., Nater, M., Goslings, D., Kessler, F., op den Camp, R., and Apel, K. (2001). FLU: a negative regulator of chlorophyll biosynthesis in Arabidopsis thaliana. Proc. Natl. Acad. Sci. USA *98*, 12826–12831.

Nakayama, T., Shinohara, H., Tanaka, M., Baba, K., Ogawa-Ohnishi, M., and Matsubayashi, Y. (2017). A peptide hormone required for Casparian strip diffusion barrier formation in Arabidopsis roots. Science *355*, 284–286.

Nawrath, C., Schreiber, L., Franke, R.B., Geldner, N., Reina-Pinto, J.J., and Kunst, L. (2013). Apoplastic diffusion barriers in Arabidopsis. Arabidopsis Book *11*, e0167.

Ohyama, K., Shinohara, H., Ogawa-Ohnishi, M., and Matsubayashi, Y. (2009). A glycopeptide regulating stem cell fate in Arabidopsis thaliana. Nat. Chem. Biol. *5*, 578–580.

Okamoto, S., Shinohara, H., Mori, T., Matsubayashi, Y., and Kawaguchi, M. (2013). Root-derived CLE glycopeptides control nodulation by direct binding to HAR1 receptor kinase. Nat. Commun. *4*, 2191.

Okuda, S., Fujita, S., Moretti, A., Hohmann, U., Doblas, V.G., Ma, Y., Pfister, A., Brandt, B., Geldner, N., and Hothorn, M. (2020). Molecular mechanism for the recognition of sequence-divergent CIF peptides by the plant receptor kinases GSO1/SGN3 and GSO2. Proc. Natl. Acad. Sci. USA *117*, 2693–2703.

Penfield, S., Li, Y., Gilday, A.D., Graham, S., and Graham, I.A. (2006). Arabidopsis ABA INSENSITIVE4 regulates lipid mobilization in the embryo and reveals repression of seed germination by the endosperm. Plant Cell *18*, 1887–1899.

Penfield, S., Rylott, E.L., Gilday, A.D., Graham, S., Larson, T.R., and Graham, I.A. (2004). Reserve mobilization in the Arabidopsis endosperm fuels hypocotyl elongation in the dark, is independent of abscisic acid, and requires phosphoenolpyruvate CARBOXYKINASE1. Plant Cell *16*, 2705–2718.

Petricka, J.J., Winter, C.M., and Benfey, P.N. (2012). Control of Arabidopsis root development. Annu. Rev. Plant Biol. *63*, 563–590.

Pfister, A., Barberon, M., Alassimone, J., Kalmbach, L., Lee, Y., Vermeer, J.E., Yamazaki, M., Li, G., Maurel, C., Takano, J., et al. (2014). A receptor-like kinase mutant with absent endodermal diffusion barrier displays selective nutrient homeostasis defects. eLife *3*, e03115.

Pineau, B., Dubertret, G., Joyard, J., and Douce, R. (1986). Fluorescence properties of the envelope membranes from spinach chloroplasts. Detection of protochlorophyllide. J. Biol. Chem. *261*, 9210–9215.

Piskurewicz, U., and Lopez-Molina, L. (2011). Isolation of genetic material from Arabidopsis seeds. Methods Mol. Biol. *773*, 151–164.

Piskurewicz, U., and Lopez-Molina, L. (2016). Basic techniques to assess seed germination responses to abiotic stress in Arabidopsis thaliana. Methods Mol. Biol. *1398*, 183–196.

Schindelin, J., Arganda-Carreras, I., Frise, E., Kaynig, V., Longair, M., Pietzsch, T., Preibisch, S., Rueden, C., Saalfeld, S., Schmid, B., et al. (2012). Fiji: an open-source platform for biological-image analysis. Nat. Methods *9*, 676–682.

Schreiber, L., and Schönherr, J. (2009). Water and Solute Permeability of Plant Cuticles (Springer).

Shinohara, H., and Matsubayashi, Y. (2013). Chemical synthesis of Arabidopsis CLV3 glycopeptide reveals the impact of hydroxyproline arabinosylation on peptide conformation and activity. Plant Cell Physiol. *54*, 369–374.

Szczuka, E., and Szczuka, A. (2003). Cuticle fluorescence during embryogenesis of Arabidopsis thaliana (L.) Heynh. . Acta Biol. Cracoviensis S. Bot. *45*, 63–67.

Tanaka, T., Tanaka, H., Machida, C., Watanabe, M., and Machida, Y. (2004). A new method for rapid visualization of defects in leaf cuticle reveals five intrinsic patterns of surface defects in Arabidopsis. Plant J. *37*, 139–146.

Tsuwamoto, R., Fukuoka, H., and Takahata, Y. (2008). GASSHO1 and GASSHO2 encoding a putative leucine-rich repeat transmembrane-type receptor kinase are essential for the normal development of the epidermal surface in Arabidopsis embryos. Plant J. *54*, 30–42.

Voisin, D., Nawrath, C., Kurdyukov, S., Franke, R.B., Reina-Pinto, J.J., Efremova, N., Will, I., Schreiber, L., and Yephremov, A. (2009). Dissection of the complex phenotype in cuticular mutants of Arabidopsis reveals a role of SERRATE as a mediator. PLoS Genet. *5*, e1000703.

Wu, X., Dabi, T., and Weigel, D. (2005). Requirement of homeobox gene STIMPY/WOX9 for Arabidopsis meristem growth and maintenance. Curr. Biol. *15*, 436–440.

Zolman, B.K., Silva, I.D., and Bartel, B. (2001). The Arabidopsis pxa1 mutant is defective in an ATP-binding cassette transporter-like protein required for peroxisomal fatty acid beta-oxidation. Plant Physiol. *127*, 1266–1278.

STAR★METHODS

KEY RESOURCES TABLE

REAGENT or RESOURCE	SOURCE	IDENTIFIER
Chemicals, peptides, and recombinant proteins		
Toluidine Blue	Thermo Fisher Scientific	Cat#89640
osmium tetroxide	Polysciences	Cat#18814
glutaraldehyde	Polysciences	Cat# 01909
Tween-20	Thermo Fisher Scientific	Cat# 93773
uranyl acetate	Merck	Cat#8473
Epon 812	Sigma-Aldrich	Cat#45345
Reynolds lead nitrate	Sigma-Aldrich	Cat#L6258
Sodium tri citrate	Thermo Fisher Scientific	Cat#71405
Sodium methoxide 256	Sigma-Aldrich	Cat#156256
Methylheptadecanoate	Sigma-Aldrich	Cat#H4515
pentadecalacton	Sigma-Aldrich	Cat#W2840009
Dichloromethane	Sigma-Aldrich	Cat#650463
N, O- bis(trimethysilyl)-trifluoroacetamide with trimethylchlorosilane (BSTFA)	Sigma-Aldrich	Cat#15238
Pyridine	Sigma-Aldrich	Cat#270970
Sodium methoxide	Sigma-Aldrich	Cat#156256
Xylitol	Sigma-Aldrich	Cat#X3375
Urea	Merck	Cat#84308
Calcolfluor white	Sigma-Aldrich	Cat#F3543
CIF2 sulfated	D(**Y**)GHSS(**P**)K(**P**)KLVRPPFKLIPN	Synthesized by Peptide Specialty Laboratories GmbH (Germany)
CIF2 unsulfated	DYGHSS(**P**)K(**P**)KLVRPPFKLIPN	Synthesized by Peptide Specialty Laboratories GmbH (Germany)
Deposited data		
RNA-seq	This study	SRA: PRJNA763191
LC-MS/MS raw data	This study	ProteomeXchange: PXD028576
Experimental models: Organisms/strains		
Arabidopsis: tpst-1	Komori et al., 2009	SALK_009847
Arabidopsis: sgn2-1	Doblas et al., 2017	EMS screen
Arabidopsis: psy1-1	This study	GK-583C09
Arabidopsis: psy1-2	This study	SALK_015322
Arabidopsis: psy1r-1	Amano et al., 2007	SALK_072802
Arabidopsis: psy1r-2	This study	SALKseq_48601
Arabidopsis: cif1-2/cif2-2	Okuda et al., 2020	N/A
Arabidopsis: cif2-2	This study	Obtained by backcrossing *cif1cif2* with WT
Arabidopsis: cif2-3	This study	N/A
Arabidopsis: pxa1-1	Zolman et al., 2001	CS3950
Arabidopsis: bdg-1	Kurdyukov et al., 2006	W32 mutant
Arabidopsis: lacs2-3	Bessire et al., 2007	GK-368C02
Arabidopsis: gpat4/gpat8	Li et al., 2007	SALK_106893; SALK_095122
Arabidopsis: rgf7	This study	SALK_077237
Arabidopsis: psy3	Luhua et al., 2013	SALK_096481
Arabidopsis: psk1	This study	SALK_063177
Arabidopsis: psk3	This study	SALK_030767

(*Continued on next page*)

Continued

REAGENT or RESOURCE	SOURCE	IDENTIFIER
Oligonucleotides		
For all oligonucleotides used for genotyping	See Table S3	N/A
Software and algorithms		
Fiji	Schindelin et al., 2012	RRID: SCR_002285
Prism GraphPad	GraphPad	RRID: SCR_002798
Cufflinks program and Cuffdiff program	Blankenberg et al., 2010; Giardine et al., 2005; Goecks et al., 2010	RRID:SCR_ 013307; RRID:SCR_001647
Xcalibur software	Thermo Fisher Scientific	RRID:SCR_014593
Imaging code	This study	Zenodo repository https://doi.org/10.5281/zenodo.5507465

RESOURCE AVAILABILITY

Lead contact

Further information and requests for resources and reagents may be directed to and will be fulfilled by Luis Lopez-Molina (luis.lopezmolina@unige.ch).

Materials availability

All new materials generated in this study will be available upon request from Luis Lopez-Molina (luis.lopezmolina@unige.ch).

Data and code availability

- The RNA-Seq raw data have been deposited at Sequence Read Archive (SRA) under accession number PRJNA763191 (SRA:PRJNA763191). The LC-MS/MS raw data has been deposited to the ProteomeXchange Consortium via the PRIDE partner repository with the dataset identifier PRIDE: PXD028576.
- The code for imaging analysis has been deposited in the Zenodo repository (Zenodo: https://doi.org/10.5281/zenodo.5507465).
- Any additional information required to reanalyze the data reported in this paper is available from the lead contact upon request.

EXPERIMENTAL MODEL AND SUBJECT DETAILS

Plant material and growth conditions

tpst-1 (SALK_009847) and *sgn2-1* were previously described by Komori et al. and Doblas et al., respectively (Doblas et al., 2017; Komori et al., 2009). The *psy1-1* allele (GK-583C09, referred as *psy1*) has a T-DNA insertion in the second exon. The *psy1-2* allele (SALK_015322) has a T-DNA insertion ~100 bp upstream of the transcription start site. *The psy1r* allele (SALK_72802) was previously described by Amano et al. (Amano et al., 2007). The *psy1r-2* allele is the SALKseq_48601 line bearing a T-DNA exon insertion. The *cif1-2* (referred as *cif1*) and *cif2-2* (referred as *cif2*) alleles in *cif1cif2* double mutants (referred as *cif1/2*) were described in Okuda et al (Okuda et al., 2020). *cif2* was obtained by crossing *cif1/2* with WT (Col-0). *cif2-3* has a 5 bp deletion in the peptide coding region of *CIF2* (2680-2685 of AT4G34600) generated by CRISPR-Cas9 as described by Okuda et al. using the 5'- gctttggtttaggactggag- 3' primer (Okuda et al., 2020). *pxa1-1* (referred as *pxa1*) was previously described by Zolman et al. (Zolman et al., 2001). *lacs2-3* (GK-368C02, referred as *lacs2*) was described by Bessire et al. (Bessire et al., 2007), *bdg-1* (referred as *bdg*) by Kurdyukov et al. (Kurdyukov et al., 2006) and *gpat4 gpat8* (SALK_106893, SALK_095122, referred as *gpat4/8*) by Li et al. (Li et al., 2007). *rgf7* (SALK_077237), *psy3* (SALK_096481), *psk1* (SALK_063177) and *psk3* (SALK_030767) were obtained from the NASC stock center. Plants were grown at 21–23 C, 16 hr/8 h day/night photoperiod, light intensity of 80 $\mu Em^{-2}s^{-1}$, humidity of 70%.

METHODS DETAILS

Seed germination and seedling growth assays

Seed batches in this study were harvested on the same day from plants grown side by side under identical environmental conditions (22–24 °C, 100 $\mu E/m^2/s$, 16 hr/8 hr day/night photoperiod, 70% relative humidity). Seeds were sterilized and plated in standard germination plates (Piskurewicz and Lopez-Molina, 2016). Dissection procedures (see below) were performed 1h after seed imbibition in the germination plates. Undissected seeds and dissected plant material was maintained in germination plates and kept in darkness at

4°C for 4d (stratification). After stratification, germination plates were transferred to light culture chambers at 22°C for 3h and either maintained in presence or absence of light (80 μE/m^2/s, 70% relative humidity).

Dissection and grafting procedures

The seed coat along the embryonic axis (hypocotyl and radicle) was incised with a fine syringe needle (BD Micro-Fine). As this procedure may damage the embryo, the embryo was expelled from the seed by gently squeezing the surface of the seed using blunted forceps. The embryo was replaced by another embryo isolated as follows: the seed coat of a seed was punctured on its apical side using a fine syringe needle and expelled from the seed by a gentle squeeze of the seed using blunted forceps. The embryo was then gently placed inside the emptied seed using blunted forceps. The SCBA procedure was performed as described (Lee and Lopez-Molina, 2013; Lee et al., 2010; Piskurewicz and Lopez-Molina, 2016).

TBO uptake assays

We used the TBO protocol previously described (De Giorgi et al., 2015), which consists of incubating plant material for 10 min at room temperature in a 0.05% TBO + water + 0.4% Tween solution followed by a gentle wash with water to remove excess TBO from plant material. This protocol was modified by increasing either the temperature to 37°C during TBO incubation or the time of incubation (15 min).

RT-qPCR

Total RNA from 500 WT and *psy1-2* seeds 36h after stratification in presence of light was extracted as described (Piskurewicz and Lopez-Molina, 2011). Total RNAs were treated with RQ1 RNase-Free DNase (Promega, Switzerland) and reverse-transcribed using ImpromII reverse transcriptase (Promega) and oligo(dT)15 primer (Promega) according to the manufacturer's recommendations. Quantitative RT–PCR was performed using the ABI 7900HT fast real-time PCR system (Applied Biosystems, Switzerland) and Power SYBR Green PCR master mix (Applied Biosys- tems). Relative transcript levels were calculated using the comparative DCt method and normalized to the PP2A (AT1G69960) gene transcript levels. Primers used: PSY1_F: CAACCCTGTTTCCGTTTCAGGTG, PSY1_R: CAACGTTCACCATCAACAAACTCC, PP2A_F: GGACCGGAGCCAACTAGGA, PP2A_R: GCTATCCGAACTTCTGCCT CATT.

RNAseq

Total RNA was isolated from plant material 4 days after stratification cultured either in absence or presence of light. The SCBA had 100 and 25 seed coat/endosperms in absence and presence of light, respectively. Total RNA was extracted from WT endo+ seedlings, endo- seedlings and endo- seedlings arising from a SCBA. RNA concentrations were measured by Qubit Fluorometric quantification system (Thermo Fisher Scientific, Switzerland). For the mature endosperm expression data shown in Table S1, total RNA was isolated from 200 mature endosperms with the seed coat still attached dissected 36h upon seed imbibition without stratification. cDNA libraries were prepared from 200 ng total RNA using a TruSeq mRNA Library Prep Kit (Illumina, Switzerland). cDNA libraries were normalized and pooled then sequenced using HiSeq 2500 (Illumina) with single-end 100 bp reads. The RNA-Seq raw data have been deposited at Sequence Read Archive (SRA) under accession number PRJNA763191.

Gene expression profile

Transcript assembly and normalization was performed with the Cufflinks program (RRID:SCR_ 013307), and gene expression levels were calculated in FPKM (Fragments Per Kilobase of exon per Million mapped fragments) units. Differential gene expression analysis was performed by Cuffdiff (RRID:SCR_001647), a part of the Cufflinks package (Blankenberg et al., 2010; Giardine et al., 2005; Goecks et al., 2010).

Transmission electron microscopy

TEM was performed as described previously (Demonsais et al., 2020). Samples were fixed overnight at 4°C in 2.5% (v/v) glutaraldehyde and 0.01% (v/v) Tween-20 in 100 mM sodium cacodylate (pH 7) after vacuum infiltration. After a primary postfixation in 1.5% (v/v) osmium tetroxide for 2 h at 4°C and a secondary postfixation in 1% (w/v) uranyl acetate for 1 h at 4°C, they were embedded in pellets of 1.5% (w/v) agarose, dehydrated in a graded ethanol series, and embedded in Epon 812. Then, 85 nm ultra-thin sections were cut using a UCT microtome (Leica), stained with 2.5% (w/v) uranyl acetate and Reynolds lead citrate, and finally observed with a Tecnai G2 Sphera (FEI) at 120 kV, equipped with a high-resolution digital camera and using a final magnification of 11'500x. In Figure 1C, the TEM data for torpedo embryos compiled observations with three WT individuals: two having longitudinal histological sections and one having transversal sections. For the mature WT embryos, the data come from three individuals all having sagittal sections. For the WT seedlings (48h) the three individuals had all transversal sections. To compare across developmental stages the cuticle of cells that are in a comparable position, we performed the analysis using TEM pictures from similar regions in the abaxial and adaxial domains of the epidermis. All the other TEM studies concern WT and mutant endo+ and endo- seedlings studied 48h after the end of seed stratification using transversal histological sections. All sections were treated in the same way and the analysis was performed using TEM pictures taken along the entire circumference of the cotyledons, covering the adaxial and abaxial sides and their adjoining cells.

Digital warping and TBO staining quantification procedures

TBO-stained cotyledons were documented using an S6D stereomicroscope equipped with an MC120HD camera (Leica). Images were processed using the software Fiji (Schindelin et al., 2012); warping was done using the Fiji plugin BigWarp (Bogovic et al., 2016). Each cotyledon was warped to an ellipse using eight reference points evenly distributed along the cotyledon outline. Warped cotyledons were then stacked, and the median projection was calculated. The resulting image was split in its red, green and blue components; the red component was singled out, inverted and the look-up table "blue orange icb" was applied.

Quantifications of TBO staining intensity were done on the inverted red component of each warped cotyledon. Low and high thresholds were applied to eliminate reflections of the stereomicroscope light on the cotyledon surface and wounds at the cotyledon surface, respectively. The total intensity was then measured either on the whole warped cotyledon surface, or at its distal tip (Figures 4B, S6B, S6D, and S6E). Fiji macros for cuticle TEM category quantification and TBO quantification on warped cotyledons have been deposited in the Zenodo repository (https://doi.org/10.5281/zenodo.5507465)

Root development analysis

Seedlings were fixed in 4% (v/v) formaldehyde and 0.1% (v/v) TritonX-100 in phosphate buffer saline (PBS; pH 7.4) for 2h at room temperature after vacuum infiltration. After washes in PBS, they were incubated in ClearSee solution (10% [w/v] xylitol, 15% [w/v] sodium deoxycholate and 25% [w/v] urea) for a minimum of 3 days in the dark. They were then stained in 0.1% (w/v) Calcofluor White in ClearSee solution for 45 minutes at room temperature, and finally washed and mounted in ClearSee solution.

Observations were done with a DM6B microscope (Leica) equipped with a DFC9000GT sCMOS camera and a PlanApo 40x/NA 1.1 water immersion objective. Calcofluor White was excited between 375nm and 435nm and emission was collected between 450nm and 490nm. Z stacks were acquired with the smallest possible sampling frequency (voxel size 163x163x338nm3), and images were subsequently enhanced using the THUNDER Large Volume Computational Clearing algorithm (Leica), which is based on a spatial filtering method followed by a decision-mask-based deconvolution algorithm.

To determine the size of the root meristematic zone, we measured the width and length of individual cortex cells from the quiescent center shootwards. Cells with a length to width ratio inferior to 2 were considered as belonging to the meristematic zone. The cell index mentioned in Figure 6E indicates the position of each cell in the cortical lineage, index 1 being the cortical cell adjacent to the quiescent center.

Cutin analysis

Seeds and embryos dissected four hours after seed imbibition (pre-dissected embryos) were stratified for 4 days. After seed stratification, plant material was cultivated in darkness for 48h. Thereafter, cotyledons from un-dissected and dissected plant material were dissected and flash frozen and extracted in isopropanol/0.01% butylated hydroxytoluene (BHT). They were then delipidized two times (16 h, 8 h) in each of the following solvents, i.e., chloroform-methanol (2:1), chloroform-methanol (1:1), methanol with 0.01% BHT, under agitation before being dried for 3 days under vacuum. Depolymerization was performed by base catalysis (Li-Beisson et al., 2013). Briefly, dried plant samples were transesterified in 2 mL of reaction medium. 20 mL reaction medium was composed of 3 mL methyl acetate, 5 mL of 25% sodium methoxide in dry methanol and 12 mL dry methanol. The equivalents of 4 mg of methyl heptadecanoate and 4 mg of pentadecalactone/sample were added as internal standards. After incubation of the samples at 60°C for 2 h 3.5 mL dichloromethane, 0.7 mL glacial acetic acid and 1 mL 0.9% NaCl (w/v) Tris 100 mM pH 8.0 were added to each sample and subsequently vortexed for 20 s. After centrifugation (1500 g for 2 min), the organic phase was collected, washed with 2 mL of 0.9% NaCl, and dried over sodium sulfate. The organic phase was then recovered and concentrated under a stream of nitrogen. The resulting monomer fraction was derivatized with BFTSA/pyridine (1:1) at 70°C for 1 h and injected out of hexane on a HP-5MS column (J&W Scientific) in a gas chromatograph coupled to a mass spectrometer and a flame ionization detector (Agilent 6890N GC Network systems). The temperature cycle of the oven was the following: 2 min at 50°C, increment of 20°C/min to 160°C, of 2°C/min to 250°C and 10°C/min to 310°C, held for 15 min. 2 independent experiments were performed with 2-4 replicates for each genotype, respectively.

Sample preparation for mass spectrometry

Supernatant samples were filtered with Amicon Ultra-0.5ml 10k centrifugal units (Merck) to separate proteins from peptides. Protein fractions were then recovered by inverse centrifugation for evaluation of leakage from endosperm tissues. Filters were subsequently washed with 80% acetonitrile + 0.1% formic acid and 80% methanol. Wash solutions were pooled with peptide eluates and dried for LC-MS/MS analyses.

Mass spectrometry analyses

Peptide eluates were resuspended in 0.05% trifluoroacetic acid, 2% (v/v) acetonitrile, for mass spectrometry analyses. Samples were injected on an Ultimate RSLC 3000 nanoHPLC system (Dionex, Sunnyvale, CA, USA) interfaced to an Orbitrap Fusion Tribrid mass spectrometer (Thermo Scientific, Bremen, Germany). Peptides were loaded onto a trapping microcolumn Acclaim PepMap100 C18 (20 mm x 100 μm ID, 5 μm, 100Å, Thermo Scientific) before separation on a reversed-phase custom packed nanocolumn (75 μm ID × 40 cm, 1.8 μm particles, Reprosil Pur, Dr. Maisch). A flowrate of 0.25 μl/min was used with a gradient from 4 to 76% acetonitrile in 0.1% formic acid (total time: 65 min). Full survey scans were performed at a 120'000 resolution, and a top speed precursor selection strategy was applied to maximize acquisition of peptide tandem MS spectra with a maximum cycle time of 1.5s. HCD

fragmentation mode was used at a normalized collision energy of 32%, with a precursor isolation window of 1.6 m/z, and MS/MS spectra were acquired at a 15'000 resolution in the orbitrap cell. Peptides selected for MS/MS were excluded from further fragmentation during 60s. Signals corresponding to *m/z* of searched peptides were extracted in Xcalibur software (Thermo Scientific, version 4.2) and compared between samples. PSY1 peptide identity was confirmed by comparing its MS/MS spectrum with an unglycosylated peptide standard. The mass spectrometry data have been deposited to the ProteomeXchange Consortium via the PRIDE partner repository with the dataset identifier PXD028576.

Leakage control

Fifty mg of endosperm tissue was transferred in a Precellys lysing tube with 300ul of FASP buffer (4% SDS, 0.1M Tris pH 7.5, 0.1M DTT) for lysis and protein extraction with a FastPrep system. Protein concentrations of extracted tissue and supernatant protein fraction were measured by a NanoPhotometer at 280nm to evaluate leakage of proteins from endosperm to supernatant. Whole quantification of proteins present in the culture medium and mature endosperms revealed that the culture medium had about 1.5 % of the protein content in endosperm tissues, showing that contamination by endosperm cellular contents in the culture medium was minimal.

Fatty acid methyl esters (FAME) preparation and analysis

Seeds and embryos dissected one hour after seed imbibition (pre-dissected embryos) were stratified for 4 days. After stratification, embryos within seeds were dissected at different time points and harvested together with the pre-dissected embryos. For fatty acid levels determination, 25 freshly dissected embryos or pre-dissected embryos were stored at -80°C in 6-mL glass tubes containing 0.5 mL of 0.2% (w/v) butylated hydroxytoluene in methanol. Tubes were closed with a lid fitted with a disposable teflon liner (VWR, 548-0111). FAMEs were prepared by direct transesterification of entire seeds, embryos or testa. Samples were completed with 0.5 mL of 10% H_2SO_4 (v/v) in methanol and 12.5 μg of triheptadecanoate as internal standard (Sigma Aldrich). Tubes were incubated at 85 °C for one hour with a shaking every 15 min. At the end of the transesterification reaction, tubes were cooled down at room temperature and briefly span down to clean both lid and tube sides from solvents. After adding 2 mL of *n*-hexane and 1.5 mL of NaCl 0.9% (w/v), tubes were thoroughly shaken for 5 min and both phases were separated by centrifugation for 5 min at 1500 *g*. The upper organic phase was transferred to a new 6-mL glass tubes and FAME extraction was repeated two additional times with 2 mL of *n*-hexane. Combined organic phases were evaporated under a flux of nitrogen and FAMEs were resuspended in 300 μL heptane. FAME samples were transferred into crimped vials and analyzed by GC-FID.

FAMEs were separated by gas chromatography on a 30 m X 0.25 mm X 0.25 μm DB-23 column (Agilent technologies). Two microliters were injected into the injection port set at a split ratio of 30:1 and 250 °C. The initial temperature of the oven was set to 100 °C. The temperature program consisted of 2 min at 100 °C, followed by an increase up to 160 °C at 25 °C/min, and up to 250 °C at 8 °C/min. The final temperature was kept constant for 4 min. The detector temperature was set at 270°C and the data rate recording at 50 Hz. FAMEs were quantified with 5-point calibration curves directly built into the instrument software using the 37 component FAME mix (Supelco).

Fluorescence Analysis

To measure protochlorophyllide accumulation the pigments from an equal number of plants were extracted in 90% acetone. After 6 hours of the extraction, the supernatant was recovered by centrifugation, and its fluorescence spectra, excited at 440 nm, recorded with a Jasco FP-750 spectrofluorometer.

Room temperature chlorophyll fluorescence of plants undergoing the embryo-to-seedling transition was monitored with a closed camera system, FluorCam 800MF (PhotoSystems Instruments). Plants were dark adapted for 15 minutes before the measurement. The maximum quantum yield of PSII (Fv/Fm) was calculated by the ratio between the fluorescence measured in dark (Fo) and the maximum fluorescence measured during a saturating light pulse (Fm). The difference between F0 and Fm is the variable fluorescence (Fv). The PSII quantum yield under the light (ΦPSII) was measured after 5 minutes exposure to white light (180 μmol photons m-2 s-1 of PAR). A saturating pulse at the end of the light period was used to measure the maximal fluorescence in light exposed seedlings (Fm'). ΦPSII was calculated as the difference between the steady state fluorescence at the end of the light phase (Ft) and the Fm' divided by the Fm' (ΦPSII=(Fm'-Ft)/Fm') (Maxwell and Johnson, 2000). The light intensity used for the assessment of PSII activity was determined empirically by measuring ΦPSII during an increasing light intensity curve.

The NPQ was calculated as NPQ = (Fm – Fm')/ Fm' and the estimated fraction of open PS II centers based on a ''lake'' model as $qL = [(Fm' – Ft)/ (Fm' – F_O')] \cdot (Fo' – Ft)$. To measure the Fo' value the actinic light was switched off and the plants subsequently exposed to far-red light for 2 seconds to oxidize the ETC, after that, the Fo' was measured in dark (Kramer et al., 2004; Maxwell and Johnson, 2000).

QUANTIFICATION AND STATISTICAL ANALYSIS

The information about statistical tests used are indicated in the figure legends. For all the experiments, stars indicate statistically significant differences (''ns'' (not significant): $p>0.05$, ''*'': $p \leq 0.05$, ''**'': $p \leq 0.01$, ''***'': $p \leq 0.001$, ''****'': $p \leq 0.0001$). The number of biological and technical replicates used is indicated in the figure legends.